Universität
Münster

institut für
theoretische physik

Bachelor Thesis

A Neutrinophilic Dark Matter Model with a Vector Portal

by

Matias Sebastian MARTY DECKER

First Examiner
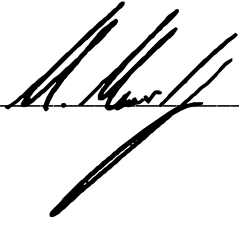Prof. Dr. Michael KLASEN

Second Examiner
PD. Dr. Karol KOVAŘÍK

University of Münster
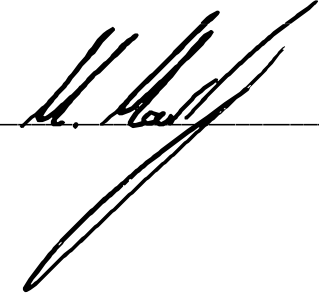Faculty of Physics
Institute of Theoretical Physics

August 29, 2024

Declaration of Academic Integrity

I hereby confirm that this thesis, entitled _A Neutrinophilic Dark Matter Model with a Vector Portal_ is solely my own work and that I have used no sources or aids other than the ones stated. All passages in my thesis for which other sources, including electronic media, have been used, be it direct quotes or content references, have been acknowledged as such and the sources cited. I am aware that plagiarism is considered an act of deception which can result in sanction in accordance with the examination regulations.

12.08.2024 ,

(date, signature of student)

I consent to having my thesis cross-checked with other texts to identify possible similarities and to having it stored in a database for this purpose.

I confirm that I have not submitted the following thesis in part or whole as an examination paper before.

12.08.2024 ,

(date, signature of student)

Abstract

Dark matter (DM), a major component of our universe whose nature remains unknown, plays a crucial role in understanding our cosmos. This thesis analyzes a neutrinophilic dark matter model featuring a proposed Dirac fermion that couples to standard model neutrinos via a vector portal. Using Feynman diagrams, the decay widths of the interaction boson and the cross sections of the annihilation processes were calculated. The model's parameters were systematically scanned to identify configurations resulting in the correct relic density and to understand how different parameters affect the final relic density. It was observed that the final relic density is proportional to the mass of the DM particle, while it is inverse proportional to the couplings. Comparison with results from `micrOMEGAs` shows that code fails at resonance but agrees within 20% in other regions. Measured neutrino fluxes from experiments were used to constrain the parameter space. These constraints indicate that the correct relic density imposes stricter limits on most of the scanned parameter space. Finally, a bisection method was introduced to optimize one parameter for fixed combinations of others. Grid scans revealed the connections between parameters necessary to achieve the correct result. Further study needs broader scans and better methods for the resonance.

Contents

Notation

For this thesis, mostly the natural units are used with $c = \hbar = k_{\mathrm{B}} = 1$. In addition to that, Greek indices (μ, $\nu \dots$) run from 0 to 3, and Latin indices (i, $j \dots$) from 1 to 3, with the Einstein summation convention applied. The time derivative is often denoted with an overdot ($dx/dt \equiv \dot{x}$). *Four-vectors* are written as a normal letter (e.g. p) and *three-vectors* are noted with an arrow above ($\vec{p}$). Also for the Feynman calculations, the slashed notation $\slashed{p} = \gamma^\mu p_\mu$ is used, among other notations discussed in the Appendix.

1 Motivation and Introduction

Since the beginning of the 20th century, controversies regarding the mass of big structures such as galaxies have risen. These controversies lead to the assumption of an additional invisible component of mass, which only interacts through gravitation. This so-called **Dark Matter** (**DM**) takes up about 27% of the universe mass-energy content. For comparison, the known ordinary matter (Baryons) only takes up a 5%. The remaining 68% is Dark Energy, which is responsible for the accelerated expansion of the universe. The true nature of Dark Matter and Dark Energy is still to be determined (p. 22 of [1]).

The best-known example of an observation that probes the existence of additional invisible matter is the rotational speed of spiral galaxies. According to classical dynamics, considering only the visible matter, the rotational speed is expected to drop with the distance to the center (red line in fig. 1.1). The observed rotational speed (green line in fig. 1.1) on the other hand, does not drop as expected.
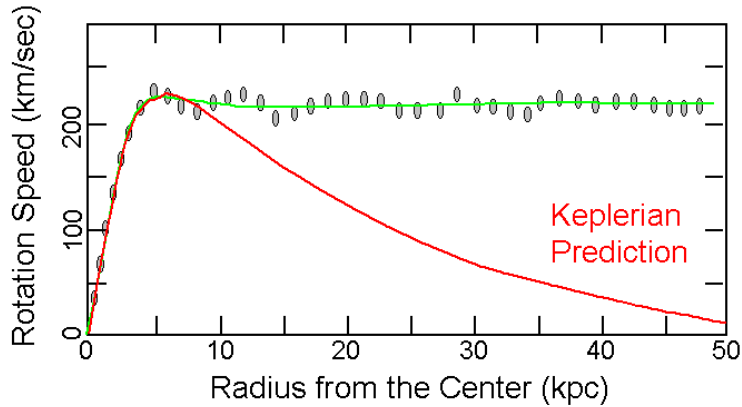

Figure 1.1: Rotation curves of spiral galaxies. The observed data is fitted with the green curve and in red is the expected rotation curve just considering the visible matter. This discrepancy is a probe for the existence of DM. (Figure taken from [2])

This phenomenon can be explained by the existence of said DM. *HW Babock* measured the rotational speed of the Andromeda Nebula, compared it to the mass distribution of the ordinary matter, and found out that in the exterior region of the galaxy there is about 60 times more DM than ordinary matter [3].

Another piece of evidence for the existence of DM comes from the observation of the Cosmic Microwave Background (CMB). It suggests that the universe is at large scales almost flat, which means that the present energy density ρ_0 is approximate to the critical density ρ_{crit} [4]. Due to this it is possible to determine the portions of the different contributions of the mass-energy content. This will be addressed later in more detail in chapter 2.2. A third very popular example for the existence of DM is inferred from the effect of gravitational lensing. According to the general theory of relativity, mass bends the fabric of space-time, and as a consequence, the straight trajectory of light
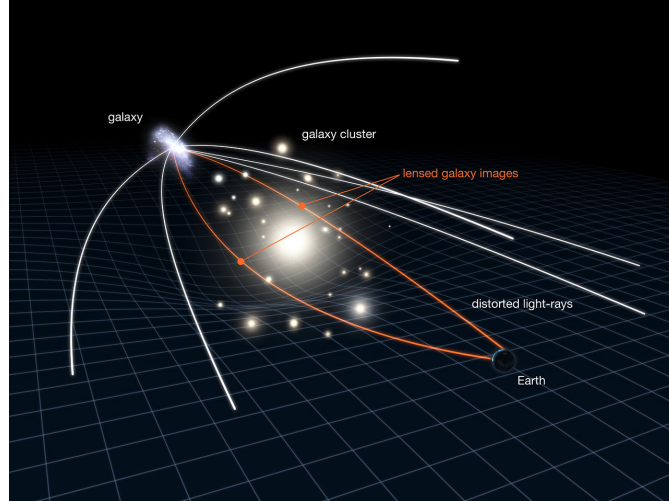
Figure 1.2: Illustration of gravitational lensing. This happens when the gravity of the object in between the galaxy and the Earth is so strong that it bends the light around itself. (Figure taken from [5])

seems to bend as well. So in the presence of a very massive object, it is possible to see light emitted behind this massive object. An illustration is shown in fig. 1.2. Since the distortion depends on the mass, it is possible to determine the mass of the massive object in between. Comparing the determined mass to the visible matter shows again that the galaxy is surrounded by more matter than "we see" [6].

In this thesis, we explore the hypothesis that dark matter (DM) can be modeled as a particle. While DM does not necessarily have to be a particle, this assumption is a prevalent and effective approach within particle physics, supported by its ability to explain various astrophysical observations and cosmological phenomena [7].

The detection of DM is divided into two parts. First the direct detection, with the goal of producing DM in a collision of known particles in a collider or measuring the recoil of visible matter due to DM scattering [8]. And second, the indirect detection. In the indirect DM search, the DM particles annihilate into Standard Model (SM) particles and the resulting flux of known particles is to be measured [9].

This Thesis analyzes a simple model in which the proposed DM particle is a Dirac fermion that couples through a vector boson to the SM specifically just to neutrinos. The goal is to explore the parameter Space set by the model consistent with today's Dm density.

It is structured in the following way: At first, the theoretical background needed to understand and derive the equations is discussed. In the Analysis and evaluation chapter, the explicit calculation of this Thesis is made, including the numerical implementation. And at the end, a conclusion and an outlook are made.

2 Theoretical Background

In this chapter, the theory needed will be explained. After a short introduction into the SM, with an emphasis on the neutrinos, the history of the universe is described in a brief way, focusing only on the relevant parts for the evaluation. A broader version is found in the Lecture Notes of Daniel Baumann [1]. The freeze-out mechanism is then presented, and the concept of relic density is introduced with the explicit example of DM decoupling. In addition to this, the Boltzmann equation for the yield and the thermally averaged cross sections are derived. Next, the Feynman rules to acquire the invariant Amplitude needed for the cross sections are depicted, and the Lorentz invariant phase space is being addressed to calculate the cross sections. Finally, the rules of how to handle the relativistic kinematics, including the Mandelstam variables, are mentioned.

2.1 The Standard Model

The Standard Model is the most current and complete description of our understanding of the particles that exist and the interactions between them. It consists of 12 fermions (six quarks and six leptons) and five bosons (four gauge bosons and the newest discovered Higgs boson). The quarks interact through a strong nuclear force, with the gluon acting as an interaction particle. Photons are the interaction particles of the electromagnetic interactions, and the Z- and W-bosons are the mediators of the weak interaction. All
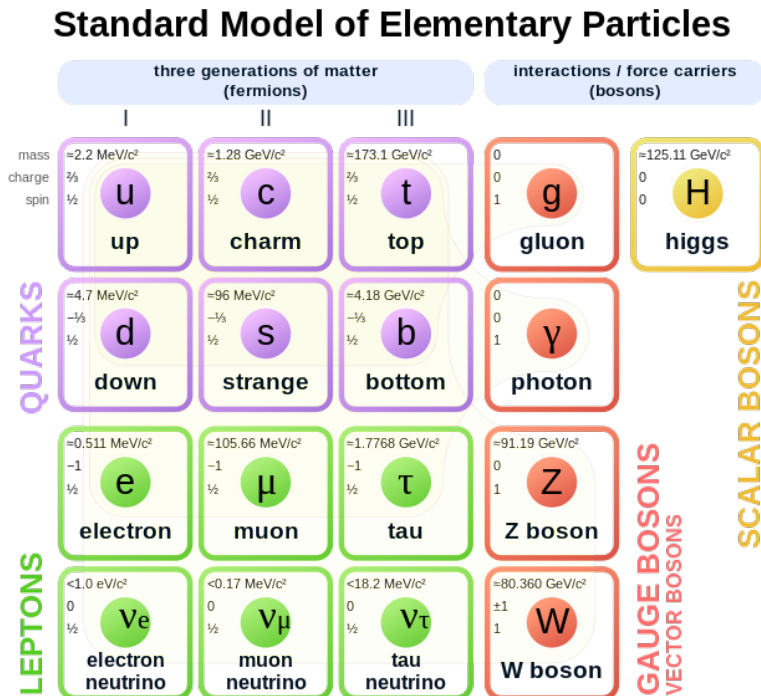

Figure 2.1: Elementary particles of the Standard Model. (Figure taken from [10])

components are shown in fig. 2.1.

The SM is a quantum field theory (QFT). This means that the particles are excitations of the different fields. QFT combines quantum mechanics with special relativity to create a more complete description, since the quantum mechanics approach fails at relativistic conditions. As a consequence, the SM fulfills the requirement of being a relativistic model. The interactions in QFT are described by a Lagrangian $\mathcal{L}$, which is a local function of the fields [11].

As only neutrinos play a role in this thesis, a further discussion of the other particles and their behaviour is omitted but can be found in detail in *Quarks and Leptons* by *Halzen and Martin* [12]

2.1.1 Neutrinos

For a long time the β-decay was believed to be a two-body decay, which leads to problems. On one hand, the energy of the emitted electron was not discrete but continuous. On the other, the angular momentum was not preserved. To ensure the conservation of angular momentum and energy in β-decays, neutrinos were first introduced by Pauli in 1930 as particles with little to no mass, spin of $\frac{1}{2}$, no electric charge and small interaction rate. Being emitted as well in the decay makes it a three-body problem, and the quantified energy can be divided between the electron and the neutrino, so a continuous spectrum is possible. The experimental proof for the existence of Neutrinos came in 1956 by Cowan and Reines in the Poltergeist experiment. The detection of neutrinos took a long time because it required a strong neutrino source due to their small interaction rates. The newly constructed nuclear power plants eventually provided this necessary source.

There is a corresponding neutrino for each of the three lepton generations (electron, muon and tau). These different types are in a superposition, so for example, an emitted electron neutrino can be detected as a muon or tau neutrino [13]. The consequence of this oscillation is that the neutrinos are not totally massless but possess a very small mass with an upper bound of $1\,\text{eV}$ for the electron neutrino as an example [14].

However, this thesis does consider the mass of neutrinos, as it is negligible compared to other masses and has minimal impact on the results. Including it would only complicate the calculations. Furthermore, this work does not differentiate between the three types of neutrinos.

2.2 Content of the Universe

For further reading and a more detailed version of the following section, Baumann's lecture notes [1] are recommended.

It is well known that the universe is expanding at an increasing rate. While the reason for this acceleration is still unknown, a mathematical description exists. To describe the expansion of the universe, the scale factor $a(t)$ is essential. Since $a(t)$ can be chosen freely, it is convention to set $a(t_0) = a_0 = 1$ (the indices 0 are used for the present).
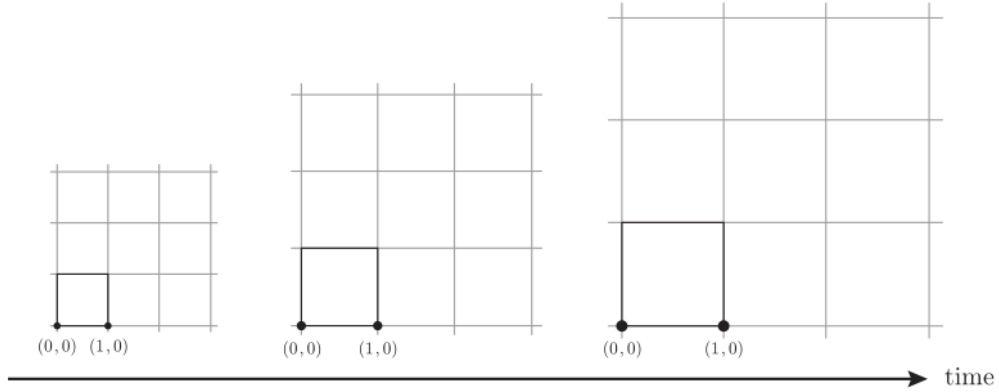
Figure 2.2: Due to the expansion of the universe there is a difference between the comoving frame and the stationary frame. In the comoving frame the distance between points is unchanged over time, but the physical distance scales with $a(t)$ and enlarges over time. (Figure taken from [1])

In fig. 2.2 the expansion is sketched, and it shows that the differentiation between the comoving frame and the physical frame is crucial. The comoving frame is an imaginary coordinate system that expands at the same rate that the universe does. In conclusion, the distance between two points in this frame remains constant. The physical distance, on the other hand, is increasing due to the expansion of the universe. Thus, the physical coordinates result in

$$r_{\text{phys}} = r\, a(t), \tag{2.1}$$

with r for the comoving coordinate. So, for example, the physical velocity is the time derivative of the physical coordinate:

$$v_{\text{phys}} = \frac{dr_{\text{phys}}}{dt} = a(t)\frac{dr}{dt} + \frac{da(t)}{dt}r = a(t)\dot{r} + Hr_{\text{phys}}. \tag{2.2}$$

H is the *Hubble Parameter*[1] and is defined as

$$H \equiv \frac{\dot{a}(t)}{a(t)}. \tag{2.3}$$

To describe the dynamics of the universe the Einstein equation

$$G_{\mu\nu} = 8\pi G T_{\mu\nu} \tag{2.4}$$

from his general relativity is used, with G the Gravitational Constant. It has the form of a tensor equation with $G_{\mu\nu}$ as the Einstein tensor and $T_{\mu\nu}$ as the stress-energy tensor, which functions as a measurement for the matter content of the universe. By observing

---

[1]Note that there is a important difference between the *Hubble Parameter H* and the *Hubble Constant* H_0. H is time dependent, where as H_0 is the value of the Hubble Parameter of today. The true value of the latter is still debated, since with different approaches the result varies between $68\,\text{km}\,\text{Mps}^{-1}\text{s}^{-1}$ and $74\,\text{km}\,\text{Mps}^{-1}\text{s}^{-1}$ [15]
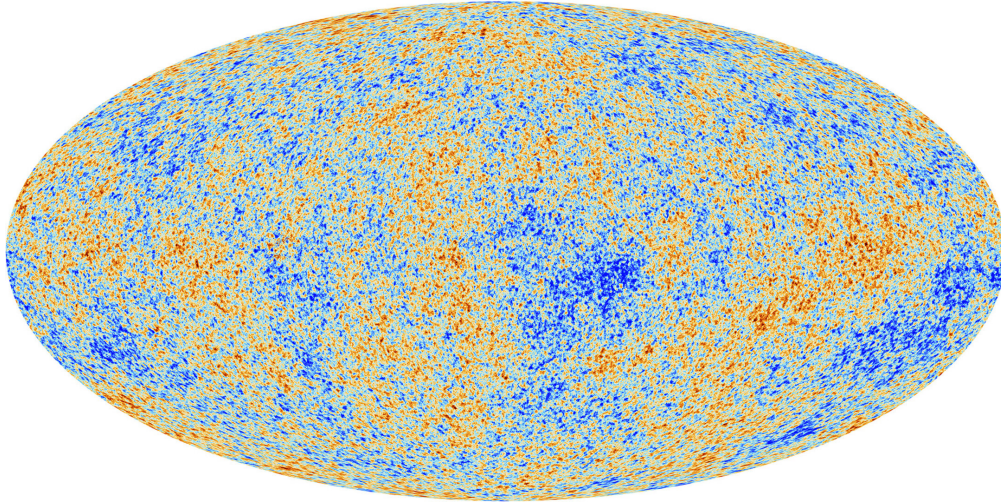
11

Figure 2.3: Cosmic microwave background as observed by Planck. On a large scale it is almost homogeneous and isotropic. (Figure taken from [16])

the CMB (fig. 2.3) it is legitimate to assume that the universe is homogeneous and isotropic on a large scale (*Cosmological principle*)[2]. With the Cosmological principle and the stress-energy tensor the continuity equation

$$\dot{\rho} + 3\frac{\dot{a}(t)}{a(t)}(\rho + P) = 0 \tag{2.5}$$

can be derived[3]. P in this equation is the pressure of the "fluid" and from now on $a(t)$ is written as a. In the ΛCDM model the universe content divides into three categories depending on the contribution to this pressure.

- **Matter**:
  Matter is the term for all non-relativistic particles with $|P| \ll \rho$. Equation 2.5 shows that for $P = 0$ the energy density

  $$\rho_{\mathrm{m}} \propto a^{-3}, \tag{2.6}$$

  which is expected, because it depends on the expansion of the volume. The contributions to the energy density of the matter is split into the contribution of ordinary matter (baryons) ρ_b and cold DM ρ_{c}.

- **Radiation**:
  Radiation is the term for relativistic particles. For these the pressure is a third of the energy density. So with equation 2.5

  $$\rho_{\mathrm{r}} \propto a^{-4} \tag{2.7}$$

---

[2]The tiny temperature fluctuations represent the marginally more dense and less dense regions of the universe. For a exact description these fluctuations need to be considered as well

[3]for the whole derivation look up the lecture notes of Baumann [1]

follows as a consequence. Due to their small mass neutrinos behaved as radiation along the history of the universe and started to behave as matter not long ago. For the energy density contributions of photons and of neutrinos ρ_γ and ρ_ν are used.

- **Dark energy**:
  As mentioned in the introduction Dark Energy will not play a role in this Thesis, but nevertheless it is still listed for completeness. Dark Energy is a negative pressure component with $P = -\rho$. This leads to

$$\rho_\Lambda \propto a^0 \tag{2.8}$$

if plugged in in equation 2.5. There is a prediction for this effect in QFT called *vacuum energy*, but this prediction is around 120 orders of magnitude away from observed.

So in total we have three contributions to the content of the universe with the proportionalities:

$$\rho \propto \begin{cases} a^{-3} & \text{matter} \\ a^{-4} & \text{radiation} \\ a^0 & \text{vacuum} \end{cases} . \tag{2.9}$$

Also the Cosmological principle simplifies the Einstein equation to two ordinary differential equations, with the first of these being known as the *first Friedmann equation*

$$H^2 = \frac{8\pi G}{3}\rho - \frac{k}{a^2}. \tag{2.10}$$

$$\Leftrightarrow \qquad H^2 = \frac{8\pi G}{3}(\rho_{\rm b}a^{-3} + \rho_{\rm c}a^{-3} + \rho_{\rm r}a^{-4} + \rho_\Lambda a^0) - \frac{k}{a^2} \tag{2.11}$$

The parameter k indicates the curvature of the universe with $k = -1$ for negative, $k = 1$ for a positive and $k = 0$ for zero curvature. For a flat universe the energy density of today is

$$\rho_{\rm crit,0} = \frac{3H_0^2}{8\pi G} = 1.9 \cdot 10^{-29}\,h^2\,\text{grams}\,\text{cm}^{-3}. \tag{2.12}$$

Using this *critical density* and the normalization for a_0, the Friedmann equation can be written as

$$\frac{H^2}{H_0^2} = \Omega_{\rm b,0}a^{-3} + \Omega_{\rm c,0}a^{-3} + \Omega_{\rm r,0}a^{-4} + \Omega_{\Lambda,0} + \Omega_{\rm k,0}a^{-2}, \tag{2.13}$$

where

$$\Omega_{\xi,0} \equiv \frac{\rho_{\xi,0}}{\rho_{\rm crit,0}}, \quad \xi = b, c, r, \Lambda \tag{2.14}$$

and

$$\Omega_{\rm k,0} \equiv \frac{-k}{(a_0 H_0)^2} \tag{2.15}$$

are dimensionless density parameters, with $\Omega_{\rm k,0}$ being a measurement for the curvature density. The values of these density parameters are obtained by the Planck experiment

under assumptions of the ΛCDM model [17]:

$$\Omega_{k,0} \leq 0.01, \quad \Omega_{b,0} = 0.05, \quad \Omega_{c,0} = 0.27, \quad \Omega_{r,0} = 9.4 \cdot 10^{-5}, \quad \Omega_\Lambda = 0.68, \quad (2.16)$$

showing that the universe is dominated by dark energy and DM (the so called dark sector). Since the contribution of the curvature today is less than 1%, and it scales with a^{-2} (compared to matter and radiation, which scale with a^{-3} and a^{-4}), it will be neglected for all times.

2.3 Thermal Equilibrium

At the beginning the universe was so dense that it was in local thermal equilibrium. Hence to describe it and its evolution the results of equilibrium thermodynamics is used. To describe the phase space density the Fermi-Dirac and Bose-Einstein distribution are used

$$\frac{g}{(2\pi)^3} \cdot f(p) = \frac{g}{(2\pi)^3} \cdot \underbrace{\frac{1}{e^{(E(p)-\mu)/T} \pm 1}}_{Fermi/Bose\ distribution}, \quad (2.17)$$

which are a result of quantum statistical mechanics. T is the temperature and μ the chemical potential. The $+$ sign applies for fermions and the $-$ sign for bosons. g are the degrees of freedom and takes the value 2 for Dirac fermions and massless vector bosons, 1 for scalar bosons and 3 for massive vector bosons. At low temperatures both distributions approach the Maxwell-Boltzmann distribution:

$$f(p) \approx e^{-(E(p)-\mu)/T} \quad (2.18)$$

For each particle species the distribution varies due to different masses and chemical potentials, where μ is negligible in the early universe.

To calculate the density of a thermodynamic parameter the integral of the phase space density multiplied by said parameter over the whole phase space needs to be performed. For the energy density this results in

$$\rho = \frac{g}{(2\pi)^3} \int d^3 p f(E) E. \quad (2.19)$$

This integral gives in the relativistic limit $(T \gg m)$

$$\rho = \frac{\pi^2}{30} g T^4 \times \begin{cases} 1 & \text{for bosons} \\ \frac{7}{8} & \text{for fermions} \end{cases}, \quad (2.20)$$

and in the non-relativistic limit $(T \ll m)$

$$\rho = g m \left(\frac{mT}{2\pi}\right)^{3/2} e^{-m/T}. \quad (2.21)$$

The conclusion is that the energy density of relativistic particles scales with T^4, while it is exponentially suppressed for non relativistic particles.

Let T be the temperature of photons. To get the radiation density (including relativistic particles) the sum over all relativistic species is performed. These don't need to be in thermal equilibrium, so each species has its own temperature T_i. So

$$\rho_r = \sum_i \rho_i = \frac{\pi^2}{30} g_{\text{eff}}(T) T^4, \tag{2.22}$$

where g_{eff} is the temperature dependent effective number of relativistic degrees of freedom. In thermal equilibrium, each species has the same temperature as the photons $T_i = T$. For this the effective degree of freedoms is

$$g_{\text{eff}}^{th}(T) = \sum_{i=\text{bos.}} g_i + \frac{7}{8} \sum_{i=\text{fer.}} g_i. \tag{2.23}$$

However a species can decouple from the thermal bath and from then on has a different temperature (see chapter 2.4). Considering this the effective degrees of freedom result in

$$g_{\text{eff}}^{dec}(T) = \sum_{i=\text{bos.}} g_i \left(\frac{T_i}{T}\right)^4 + \frac{7}{8} \sum_{i=\text{fer.}} g_i \left(\frac{T_i}{T}\right)^4. \tag{2.24}$$

In the same way g_{eff} is the effective number of degrees of freedom for the energy density, h_{eff} is the number of degrees of freedom for the entropy density

$$\tilde{s} \equiv \frac{S}{V} = \frac{2\pi^2}{45} h_{\text{eff}}(T) T^3, \tag{2.25}$$

with

$$h_{\text{eff}}^{dec}(T) = \sum_{i=\text{bos.}} g_i \left(\frac{T_i}{T}\right)^3 + \frac{7}{8} \sum_{i=\text{fer.}} g_i \left(\frac{T_i}{T}\right)^3. \tag{2.26}$$

Note that in equilibrium, when all the relativistic species have the same temperature, $h_{\text{eff}} = g_{\text{eff}}$. These conditions remain valid for $t \lesssim 1\,\text{s}$ in the early universe. The values for g_{eff} and h_{eff} are listed in tables. As a parameter to include the content of the universe

$$g_*^{1/2}(T) = \frac{h_{\text{eff}}(T)}{g_{\text{eff}}^{1/2}(T)} \left(1 + \frac{1}{3} \frac{T}{h_{\text{eff}}(T)} \frac{dh_{\text{eff}}}{d(T)T}\right) \tag{2.27}$$

is defined. The values for this combined parameter of degrees of freedom are listed in a table as well.

2.4 Freeze-Out Mechanism and Relic Density

In thermal equilibrium the *rate of interaction* Γ is higher than the *rate of expansion* H, so that equilibrium is reached before the impact of the expansion is notable. With the universe cooling down, Γ drops faster than H, until the particles decouple from the

15

thermal bath at

$$\Gamma \sim H. \tag{2.28}$$

Since the interaction rate is different between particle species, they can decouple at distinct times having individual temperatures. This is also known as the *particles freeze-out*. For clarity, in figure 2.4 the comoving number density n/T^3 is plotted against m/T, which can be seen as a measure of time (low m/T means high temperature, resulting in early times, and vice versa).
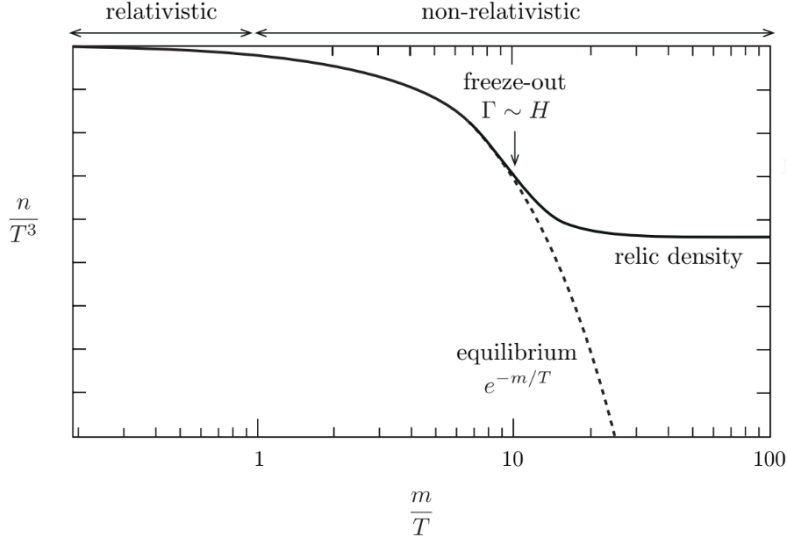

Figure 2.4: Shown is the freeze-out of an arbitrary particle species. At $\Gamma \sim H$ the freeze-out happens resulting in an almost constant relic density. (Figure taken from [1])

At high Temperatures (early times) the density follows its equilibrium value, but when the expansion rate drops below the expansion rate, the particle species decouples from the thermal bath, and the freeze out happens. This results in an almost constant comoving number density or **relic density**.

This mechanism is explained briefly using the examples of neutrinos. These are coupled to the thermal bath through weak interactions like

$$\nu_\mathrm{e} + \bar{\nu}_\mathrm{e} \leftrightarrow e^+ + e^-, \tag{2.29}$$

$$e^- + \bar{\nu}_\mathrm{e} \leftrightarrow e^- + \bar{\nu}_\mathrm{e} \tag{2.30}$$

At low temperatures, near freeze-out, the propagators of the weak interaction ($W^\pm$ and Z) acquire their masses ($M_\mathrm{W} \approx 80, \mathrm{GeV}$ and $M_\mathrm{Z} \approx 90, \mathrm{GeV}$). The cross section and interaction rate involving these weak interaction bosons are given by

$$\sigma \sim \frac{\alpha^2}{M_\mathrm{W}^4}T^2, \qquad\qquad \Gamma \sim \frac{\alpha^2}{M_\mathrm{W}^4}T^5, \tag{2.31}$$

where α is the fine-structure constant. Using $H \sim T^2/M_\mathrm{pl}$ (with M_pl being the Planck

mass), the ratio is

$$\frac{\Gamma}{H} \sim \left(\frac{T}{1\,\text{MeV}}\right)^3 . \tag{2.32}$$

This ratio falls below 1 around $T \sim 1, \text{MeV}$, marking the temperature at which neutrinos decouple from the thermal bath.[4]

The DM particle postulated in this thesis behaves similarly (see Section 3.1), allowing the relic density to be calculated for various parameter sets to determine which combinations result in the correct final relic density.

In this thesis the assumption is made that DM is a weakly interacting massive particle (*WIMP*) and the relic density is produced via freeze-out. The correct final density of the dark matter is mentioned in Section 2.2 ($\Omega_{c,0} = 0.27$). Since the density depends on the Hubble constant, whose exact value is still imprecise, it is preferable to use the form Ωh^2. Here, h represents the Hubble constant in units of $\text{km}\,\text{Mpc}^{-1}\text{s}^{-1}$, making the result independent of the exact value of the Hubble constant. Henceforth, when referring to the relic density of DM, this form will be used. The notation $\Omega_{c,0} h^2 \equiv \Omega h^2$ is adopted, indicating the relic density for cold dark matter observed today as:

$$\Omega h^2 = 0.120 \pm 0.001. \tag{2.33}$$

This value is the used to constrain the models parameter space [17].

2.4.1 Boltzmann Equation

Without any interaction the number density of a particle species i can be described with

$$\frac{1}{a^3}\frac{d(n_i a^3)}{dt} = 0. \tag{2.34}$$

This describes the conservation of the number of particles in a fixed physical volume, so that the density decreases with the expanding volume resulting in $n_i \sim a^{-3}$. The collision term

$$\frac{1}{a^3}\frac{d(n_i a^3)}{dt} = C_i[\{n_j\}] \tag{2.35}$$

is added to include the effects of collision with other particles. This is the *Boltzmann equation*. For an example

$$1 + 2 \rightleftarrows 3 + 4 \tag{2.36}$$

process

$$\frac{1}{a^3}\frac{d(n_i a^3)}{dt} = -\langle \sigma v \rangle \left[n_1 n_2 - \left(\frac{n_1 n_2}{n_3 n_4}\right)_{\text{eq}} n_3 n_4 \right] \tag{2.37}$$

can be derived, where n_i^{eq} are the equilibrium number densities and $\langle \sigma v \rangle$ is the thermally averaged cross section times velocity, which will be discussed in more detail in section 2.6.2.

---

[4]For further reading and a more detailed introduction, consult Daniel Baumann's lecture notes [1].

for the case that both, the particle species and all the species that interact with that species, are in thermal equilibrium and particle 2 is the antiparticle of particle 1

$$\dot{n} + 3Hn = -\frac{1}{2}\langle\sigma v\rangle(n^2 - n_{\text{eq}}^2) \tag{2.38}$$

can be derived [18]. To filter out the expansion of the universe a comoving number density $Y = n/\mathcal{S}$ the yield. $\mathcal{S}$ is the total entropy density of the universe. For the yield the Boltzmann equation can be derived to be

$$\dot{Y} = -\frac{\mathcal{S}}{2}\langle\sigma v_{\text{Møl}}\rangle(Y^2 - Y_{\text{eq}}^2), \tag{2.39}$$

where $v_{\text{Møl}}$ is the *Møller velocity*[5]

$$v_{\text{Møl}} = (|v_1 - v_2|^2 - |v_1 \times v_2|^2)^{1/2}. \tag{2.40}$$

With some modifications and rewriting it as a function of $x = m/T_\gamma$ the Boltzmann equation takes the form:

$$\frac{dY}{dx} = -\left(\frac{45}{\pi}G\right)^{-1/2}\frac{g_*^{1/2}m}{x^2}\frac{1}{2}\langle\sigma v_{\text{Møl}}\rangle(Y^2 - Y_{\text{eq}}^2). \tag{2.41}$$

This formulation is used in the numerical calculations presented in this thesis. The equation for the yield in equilibrium is given by:

$$Y_{\text{eq}} = \frac{45g}{4\pi^4}\frac{x^2 K_2(x)}{h_{\text{eff}}(m/x)}. \tag{2.42}$$

This equation as in the paper by Gondolo and Gelmini [18] is the non-relativistic approximation of the equilibrium yield. To calculate the final relic density some more steps need to be made. With the yield at the decoupling Y_{FO} and the freeze out temperature the resulting Yield for today Y_0 can be approximated with

$$\frac{1}{Y_0} = \frac{1}{Y_{\text{FO}}} + \left(\frac{45}{\pi}G\right)^{1/2}\int_{T_0}^{T_{\text{FO}}} g_*^{1/2}\langle\sigma v_{\text{Møl}}\rangle dT, \tag{2.43}$$

derived, which is then used to finally calculate the resulting relic density with

$$\Omega h^2 = g_{\text{D}}\frac{m_{\text{D}}Y_0\mathcal{S}_0}{\rho_{\text{crit}}}. \tag{2.44}$$

The index 0 stands for the value of today and g_{D} is the internal degrees of freedom of the DM particle [18].

---

[5]The use of the *Møller velocity* is a still discussed topic, because it does not ensure that the thermal average is invariant [19]. Nevertheless it is still used in most simulation codes, as it gives very good results if the DM is non relativistic at decoupling.

2.5 Relativistic Kinematics

At this point, it is beneficial to insert a brief interlude about relativistic kinematics and the so-called *Mandelstam variables*. The here presented equations are taken from chapter 3.2 of *Quarks and Leptons* by *Halzen and Martin* [12].

In special relativity, space and time together build the four-dimensional spacetime. To describe the energy and momentum of a particle, the *four-momentum* is used:

$$p^\mu \equiv (p^0, p^1, p^2, p^3) = (E, \vec{p}), \tag{2.45}$$

with the energy as the zeroth component. This is a contravariant vector. A covariant vector is defined as

$$p_\mu \equiv (E, -\vec{p}). \tag{2.46}$$

These *four-vectors* have specific multiplication rules. Using the Minkowski metric:

$$g_{\mu\nu} = \begin{pmatrix} 1 & 0 & 0 & 0 \\ 0 & -1 & 0 & 0 \\ 0 & 0 & -1 & 0 \\ 0 & 0 & 0 & -1 \end{pmatrix} \tag{2.47}$$

the dot product of two *four-vectors* is given by:

$$p_A \circ p_B = g_{\mu\nu} p_A^\mu p_B^\nu = p_A^\mu p_{B\mu} = (E_A E_B - \vec{p}_A \vec{p}_B), \tag{2.48}$$

with $\vec{p}_A \vec{p}_B$ being the usual scalar product of the three-momenta. If in equation 2.48 $p_A = p_B = p$, then it is obvious that the square of the momentum is:

$$p^2 = E^2 - \vec{p}^2 = m^2, \tag{2.49}$$

making use of the relativistic energy-momentum relation. For a scattering process, let the four-momenta of the incoming particles be p_A and p_B, and for the outgoing particles k_1 and k_2. The first Mandelstam variable is the invariant mass squared:

$$s = (p_A + p_B)^2 = (k_1 + k_2)^2. \tag{2.50}$$

In a similar way, the other Mandelstam variables are defined as:

$$t = (p_A - k_1)^2 = (p_B - k_2)^2, \tag{2.51}$$

$$u = (p_A - k_2)^2 = (p_B - k_1)^2. \tag{2.52}$$

These variables are Lorentz invariant and fulfill the relation:

$$s + t + u = m_A^2 + m_B^2 + m_1^2 + m_2^2. \tag{2.53}$$

The Mandelstam variables are essential in describing the kinematics of particle collisions. They simplify the analysis of scattering processes because they remain invariant under Lorentz transformations, ensuring that physical predictions do not depend on the reference frame (page 94 in [12]).

2.6 Cross Sections

Before the earlier mentioned thermally averaged cross section times velocity ($\langle \sigma v \rangle$) is discussed, we'll define what a cross section in general is and how it can be calculated using the *Feynman diagrams*. The cross section is a measurement for the probability that an interaction happens between particles. It has the unit of an area, which can be seen as a collision area. If the area increases, so does the probability for an interaction.

2.6.1 Cross Section from Feynman Diagrams

The Feynman diagrams and the Feynman rules are shown in detail in appendix B. Said diagrams are graphical descriptions of mathematical terms used to calculate the matrix element $\mathcal{M}_{\mathrm{fi}} = \langle f | U | i \rangle$ essential to get the cross section. For example, incoming fermions are depicted as an incoming arrow, and incoming antifermions as an outgoing arrow (because they can be described as fermion moving back in time):

$$\tag{2.54}$$

The point where these lines intersect is called vertex. Here the couplings come into play, because they are a measurement of how strong the interaction is at that vertex. The interaction bosons have different symbols. As an example the Feynman diagram of an annihilation of two incoming particles with the four-momentum p_A and p_B into two outgoing particles with the four-momenta k_1 and k_2 through a interaction particle γ looks like this:

$$\tag{2.55}$$
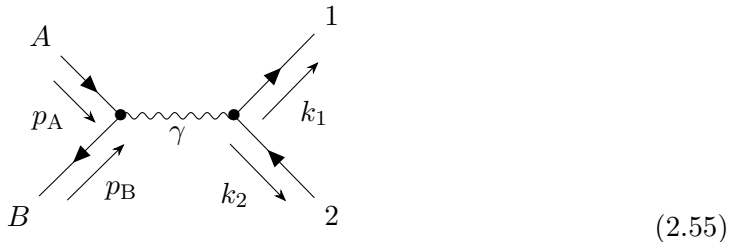
These Feynman diagrams can represent different orders of the annihilation, and in this thesis just the leading order, meaning the simplest diagrams will be considered. U is the time evolution operator to calculate the change of the system from the initial state $|i\rangle$ to the final state $\langle f|$ in time. With the matrix element the *invariant amplitude* $|\overline{\mathcal{M}}|^2$ can be calculated and with

$$\frac{d\sigma}{d\Omega} = \frac{\alpha}{64\pi^2 s} \frac{|\vec{p}_f|}{|\vec{p}_i|} |\overline{\mathcal{M}}|^2 \tag{2.56}$$

the differential cross section in the cms is obtained [12]. Here Ω is the solid angle and $\vec{p}_i (\vec{p}_f)$ is the momentum of the incoming (outgoing) particles and α takes the value $1/2$ if the outgoing particles are identical. To calculate $|\overline{\mathcal{M}}|^2$ we have to sum over the possible outgoing states and average over all possible initial states. Hence for a $A + B \rightarrow 1 + 2$ process, where the initial particles have the spin J_a and J_b:

$$|\overline{\mathcal{M}}|^2 = \frac{1}{(2J_a + 1)(2J_b + 1)} \sum_{i,f} |\mathcal{M}_{fi}|^2. \tag{2.57}$$

Analogously the decay width can be calculated with:

$$\Gamma_{A \rightarrow 1+2} = \alpha \frac{|\vec{p}_f|}{32\pi^2 m_A^2} \int |\overline{\mathcal{M}}|^2 d\Omega, \tag{2.58}$$

for a particle A decaying into two particles $1 + 2$ (equation 4.37 in [12]).

The differential cross section in the expressed form of equation 2.56 is not Lorentz invariant, because the angles change under transformation. To get a Lorentz invariant expression for the cross section the scattering angle is substituted with the Mandelstam variable t. To do so t needs to be rewritten as

$$\begin{aligned} t &= (p_A - k_1)^2 = p_A^2 - 2p_A k_1 + k_1^2 \\ &= m_A^2 - 2(E_A E_1 - \vec{p}_A \vec{k}_1) + m_1^2 \\ &= m_A^2 - 2E_A E_1 + 2|\vec{p}_A||\vec{k}_1| \cos\vartheta + m_1^2, \end{aligned} \tag{2.59}$$

with ϑ as cms scattering angle. This is the polar angle between the particles A and 1. Also the Energies and three-momenta of the particles in the center-of-momentum frame can be rewritten as

$$E_A = \frac{s + m_A^2 - m_B^2}{2\sqrt{s}} \qquad\qquad E_B = \frac{s + m_B^2 - m_A^2}{2\sqrt{s}}$$

$$E_1 = \frac{s + m_1^2 - m_2^2}{2\sqrt{s}} \qquad\qquad E_2 = \frac{s + m_2^2 - m_1^2}{2\sqrt{s}} \tag{2.60}$$

$$|\vec{p}_{A,B}| = \frac{1}{2\sqrt{s}} \lambda^{1/2}(s, m_A^2, m_B^2) \qquad |\vec{p}_{1,2}| = \frac{1}{2\sqrt{s}} \lambda^{1/2}(s, m_1^2, m_2^2). \tag{2.61}$$

Here λ the Källén function

$$\lambda(s, m_1, m_2) = (s - m_1^2 - m_2^2)^2 - 4m_1^2 m_2^2, \tag{2.62}$$

also known as triangle function is used. Using equations 2.60 and 2.61 the differential cross section takes the form

$$\frac{d\sigma}{dt} = \frac{1}{16\pi\lambda(s, m_A^2, m_B^2)} |\overline{\mathcal{M}}|^2. \tag{2.63}$$

The fraction in front of the invariant Amplitude is also referred to as *Flux-Factor*. By integrating this expression the total cross section can be calculated

$$\sigma_{A+B\to 1+2} = \int_{t_-}^{t_+} \frac{1}{16\pi\lambda(s, m_A^2, m_B^2)} |\overline{\mathcal{M}}|^2 dt, \tag{2.64}$$

with

$$t_\pm = m_A^2 + m_1^2 - \frac{(s - m_A^2 + m_B^2)(s - m_1^2 + m_2^2)}{2s} \pm \frac{1}{2s} \lambda^{1/2}(s, m_A^2, m_B^2)\lambda^{1/2}(s, m_1^2, m_2^2). \tag{2.65}$$

In this Thesis equation 2.64 is used to obtain the total cross sections. For a more detailed derivation of the final integral for the total cross section and the integral bounds see [20][21][22]

2.6.2 Thermally Averaged Cross Section

In the Boltzmann equation for the yield 2.41 the thermally averaged cross section times the Møller velocity appears, which is defined as

$$\langle \sigma v_{\text{Møl}} \rangle = \frac{\int \sigma v_{\text{Møl}} \, dn_A^{\text{eq}} \, dn_B^{\text{eq}}}{\int dn_A^{\text{eq}} \, dn_B^{\text{eq}}}. \tag{2.66}$$

The equilibrium distribution function, which is the Fermi-Dirac-distribution for fermions and the Bose-Einstein-distribution for bosons, can be approximated by the Maxwell-Boltzmann equation. This is a good approximation for $x \gtrsim 1/3$, and since in this Thesis the Boltzmann equation is solved from $x = 1$ the thermal averaged cross section concludes to

$$\langle \sigma v_{\text{Møl}} \rangle = \frac{\int \sigma v_{\text{Møl}} \, e^{-E_A/T} e^{-E_B/T} \, d^3 \vec{p}_A \, d^3 \vec{p}_B}{\int e^{-E_A/T} e^{-E_B/T} \, d^3 \vec{p}_A \, d^3 \vec{p}_B}. \tag{2.67}$$

Using spherical coordinates to describe the momentum-space volume element in terms of the Energies of the particle and the relative angle between them, results in:

$$d^3 \vec{p}_A \, d^3 \vec{p}_B = 4\pi |\vec{p}_A| E_A dE_A \, 4\pi |\vec{p}_B| E_B dE_B \, \frac{1}{2} \, d\cos\vartheta. \tag{2.68}$$

With the substitution of

$$E_\pm = E_A \pm E_B \tag{2.69}$$

$$s = m_A^2 + 2E_A E_B - 2|\vec{p}_A||\vec{p}_B|\cos\vartheta + m_B^2, \tag{2.70}$$

equation 2.68 becomes

$$d^3\vec{p}_A\, d^3\vec{p}_B = 2\pi^2 E_A E_B dE_+ dE_- ds. \tag{2.71}$$

Plugging this into equation 2.67 and doing some reshaping the final expression for the thermally averaged cross section times Møller velocity is derived to be

$$\langle \sigma v_{\text{Møl}} \rangle = \frac{x}{8m^5 K_2^2(x)} \int_{4m^2}^\infty ds\, \sigma(s - 4m^2)\sqrt{s} K_1\left(\frac{\sqrt{s}x}{m}\right). \tag{2.72}$$

K_i is the modified Bessel function of the i-th kind. This expression applies for particles that follow the Maxwell-Boltzmann distribution. As mentioned earlier this will be the only case treated in this thesis [18].

2.6.3 Non-relativistic thermal averaging

To later recast the limits on the parameter space set by the experiments that measure the neutrino Flux it is necessary to expand the thermally averaged cross section in powers of the velocity:

$$\langle \sigma v \rangle = a + b\langle v^2 \rangle + \mathcal{O}(v^4). \tag{2.73}$$

This can be used as a non-relativistic approximation, where $\langle v^2 \rangle$ is the averaging over the DM velocity at the signal source. To get the for the constraints relevant *s-wave* (*a*) and *p-wave* (*b*) contribution the Mandelstam variable s needs to be expanded and approximated as

$$s = m_A^2 + m_B^2 + \frac{m_A^2 + m_B^2}{\sqrt{1 - v^2}} \approx (2m_A^2 + 2m_B^2)\left(1 + \frac{v^2}{4}\right). \tag{2.74}$$

If

$$\epsilon \equiv \frac{s - (2m_A + 2m_B^2)}{(2m_A + 2m_B^2)} \tag{2.75}$$

is plugged into equation 2.74 the velocity can be calculated as

$$v = \frac{2\sqrt{\epsilon(1 + \epsilon)}}{1 + 2\epsilon} \tag{2.76}$$

The expansion of the thermally averaged cross section is given by

$$\sigma v = \sum_{n=0}^\infty \frac{a^{(n)}}{n!}\epsilon^n = a^{(0)} + a^{(1)}\epsilon + \frac{1}{2}a^{(2)}\epsilon^2 + \dots, \tag{2.77}$$

23

where $a^{(n)}$ represents the n-th derivation with respect to ϵ of σv at $\epsilon = 0$. With the definition of ϵ the expansion is

$$\sigma v = a^{(0)} + a^{(1)} \left(\frac{v^2}{4} \right) + \frac{1}{2} a^{(2)} \left(\frac{v^4}{16} \right) + \cdots . \tag{2.78}$$

The *s-wave* contribution is the first expansion factor $(a = a^{(0)})$ and for the *p-wave* contribution the second factor is used $(b = a^{(1)}/4)$. Since the constraints for the parameter space set by the *p-wave* contribution are normally less strict than the constraints set by the *s-wave* contribution only latter will be regarded in this Thesis [18].

3 Analysis and Evaluation

In this section, the theoretical background discussed is used to obtain some results. First, the model used for the DM candidate is presented, along with its Lagrangian, which is only used to obtain the processes that come along with the proposed model. The Feynman diagrams and rules are then employed to calculate the cross sections and decay rates. Additionally, the calculation for the non-relativistic approximation is presented. This is done, because neutrino flux experiments around the globe can set upper limits for this approximation, which can be transferred to constraints on the parameter space of the model (since the the DM particle couples to neutrinos only). Following the analytical calculations, the numerical solution of the Boltzmann equation 2.41 is performed in order to calculate the final relic density for different sets of parameters. Finally, a bisection method is presented as a final step in the process, allowing for the optimal value of a parameter to be identified, ensuring that the calculated relic density is always correct.

3.1 Model for Dark Matter

The model for Dark Matter in this thesis consists of the Standard Model (SM) as the visible sector and proposes a hidden sector including a Dark Matter particle D and its antiparticle $\bar{D}$, both with masses m_D. These particles are Dirac fermions, thus having spin $\frac{1}{2}$. Additionally, a vector boson Z' with mass $M_{Z'}$ serves as a portal between the hidden and visible sectors. The Z'-portal couples exclusively to the neutrinos of the visible sector. The total Lagrangian of this model can be written as

$$\mathcal{L} = \mathcal{L}_\mathrm{SM} + \mathcal{L}_\mathrm{kin} + \mathcal{L}_\mathrm{int}. \tag{3.1}$$

To the already known Lagrangian of the SM, two additional terms are included: the free Lagrangian and the interactions of the hidden sector. These are given by

$$\mathcal{L}_\mathrm{kin} = -\frac{1}{4}Z'_{\mu\nu}Z'^{\mu\nu} + \frac{1}{2}M_{Z'}^2 Z'_\mu Z'^\mu + \bar{D}(i\gamma^\mu \partial_\mu - m_\mathrm{D})D, \tag{3.2}$$

$$\mathcal{L}_\mathrm{int} = -\bar{\nu}_i \gamma^\mu (g_{ij} - g'_{ij}\gamma_5)Z'_\mu \nu_j - g_X \bar{D}\gamma^\mu(1-\gamma_5)Z'_\mu D. \tag{3.3}$$

Here, γ_5 is the fifth Dirac matrix (see appendix A), which is needed for the mathematical description that only left-chiral particles participate in weak interactions. g_{ij} and g'_{ij} are the coupling constants that measure the strength of the interactions of the hidden sector that are coupled to neutrinos. For simplicity, these are assumed to be diagonal, so $g_{ij} = g\delta_{ij}$ and $g'_{ij} = g'\delta_{ij}$. As a result, the three neutrino flavors are treated equally in the $Z' \leftrightarrow \nu\bar{\nu}$ vertex, and no flavor changing occurs between the three neutrino types. From the Lagrangians in equations 3.2 and 3.3, the following processes can be derived:

- The term $-\bar{\nu}_i\gamma^\mu(g_{ij} - g'_{ij}\gamma_5)Z'_\mu\nu_j$ encodes the interaction between the portal and the neutrinos. From this, the decay $Z' \to \nu\bar{\nu}$ can be extracted.

- The term $g_X \bar{D} \gamma^\mu (1 - \gamma_5) Z'_\mu D$ describes the interaction within the dark sector, and the decay $Z' \to D\bar{D}$ can be derived.

- Using both vertices described by the Lagrangian, two annihilation processes are possible:

  1. $D\bar{D} \to \nu\bar{\nu}$
  2. $D\bar{D} \to Z'Z'$

In the following sections, the cross sections of these processes are calculated to determine the final relic density.

3.2 Calculated Cross Sections and Decay Widths

Here, the explicit calculations to obtain the invariant amplitude of the Z' decays and the annihilation processes are shown using Feynman diagrams and rules (a short list of the Feynman rules are in appendix B). These calculations are then used to derive decay width of the portal and the cross sections of the annihilation processes. Note that in the following calculations, the distinction between contravariant and covariant indices is ignored, as the correct application of Feynman rules ensures proper results. Therefore all indices are noted as superposition (appart from γ_5). also important to mention is that some steps of the calculation were performed using the *FeynCalc* package in `MATHEMATICA` 13 [23].

3.2.1 Z' Decays

For this first calculation the steps are noted more detailed than in the later processes, as the procedure is similar and can be transferred to the other terms.
The diagram for the first Decay is:

$$(3.4)$$
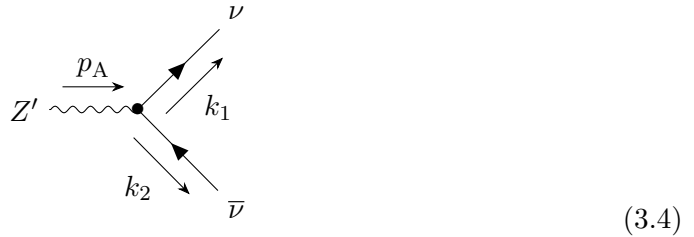
For the incoming Z'-vector boson, the Feynman rule is $\varepsilon_\lambda(p_A)$. The outgoing neutrino is noted as $\bar{u}_\nu^{(s_1)}(k_1)$ and the antineutrino as $v_\nu^{(s_2)}(k_2)$, where ν in the index refers to the neutrino and is not summed over. From the Lagrangian in equation 3.3, the interaction term for the $Z' \leftrightarrow \nu\bar{\nu}$ vertex can be derived as $i\gamma^\mu(g - g'\gamma_5)$. Applying the rules for spinors and Dirac-matrices (see appendix A for the Dirac-matrix rules) the chain follows

26

to be

$$\mathcal{M} = \varepsilon_\lambda^\mu(p_A)\bar{u}_\nu^{(s_1)}(k_1)i\gamma^\mu(g - g'\gamma_5)v_\nu^{(s_2)}(k_2)$$
$$= i\varepsilon_\lambda^\mu(p_A)u_\nu^{\dagger(s_1)}(k_1)\gamma^0\gamma^\mu(g - g'\gamma_5)v_\nu^{(s_2)}(k_2), \tag{3.5}$$

where the parenthesised superscription denotes the spin of the different particles. To obtain the absolute square ($|\mathcal{M}|^2 = \mathcal{M}\mathcal{M}^\dagger$) the hermitian adjoint

$$\mathcal{M}^\dagger = \left[i\varepsilon_\lambda^\nu(p_A)u_\nu^{\dagger(s_1)}(k_1)\gamma^0\gamma^\nu(g - g'\gamma_5)v_\nu^{(s_2)}(k_2)\right]^\dagger$$
$$= v_\nu^{\dagger(s_2)}(k_2)(g - g'\gamma_5)^\dagger\gamma^{\nu\dagger}\gamma^{0\dagger}u_\nu^{(s_1)}(k_1)(-i)\varepsilon_\lambda^{*\nu}(p_A) \tag{3.6}$$

is needed. Making use of:

$$\gamma^{\nu\dagger} = \gamma^0\gamma^\nu\gamma^0 \quad \text{and} \quad \gamma^{0\dagger} = \gamma^0 \tag{3.7}$$

it concludes to

$$\mathcal{M}^\dagger = -iv_\nu^{\dagger(s_2)}(k_2)(g - \gamma_5 g')\gamma^0\gamma^\nu\gamma^0\gamma^0 u_\nu^{(s_1)}(k_1)\varepsilon_\lambda^{*\nu}(p_A)$$
$$= -iv_\nu^{\dagger(s_2)}(k_2)(g - \gamma_5 g')\gamma^0\gamma^\nu 1 u_\nu^{(s_1)}(k_1)\varepsilon_\lambda^{*\nu}(p_A). \tag{3.8}$$

Because γ_5 anticommutes with the other γ-matrices, when the remaining γ^0 is passed to the other side of the parenthesis the sign changes from $-$ to $+$ inside the parenthesis:

$$\Rightarrow \mathcal{M}^\dagger = -iv_\nu^{\dagger(s_2)}(k_2)\gamma^0(g + \gamma_5 g')\gamma^\nu u_\nu^{(s_1)}(k_1)\varepsilon_\lambda^{*\nu}(p_A)$$
$$= -i\bar{v}_\nu^{(s_2)}(k_2)(g + \gamma_5 g')\gamma^\nu u_\nu^{(s_1)}(k_1)\varepsilon_\lambda^{*\nu}(p_A)$$
$$= -i\bar{v}_\nu^{(s_2)}(k_2)(g + g'\gamma_5)\gamma^\nu u_\nu^{(s_1)}(k_1)\varepsilon_\lambda^{*\nu}(p_A). \tag{3.9}$$

So the amount square concludes to be

$$|\mathcal{M}|^2 = \mathcal{M}\mathcal{M}^\dagger$$
$$= \left[\varepsilon_\lambda^\mu(p_A)\bar{u}_\nu^{(s_1)}(k_1)i\gamma^\mu(g - g'\gamma_5)v_\nu^{(s_2)}(k_2)\right]\left[-i\bar{v}_\nu^{(s_2)}(k_2)(g + g'\gamma_5)\gamma^\nu u_\nu^{(s_1)}(k_1)\varepsilon_\lambda^{*\nu}(p_A)\right]$$
$$= \varepsilon_\lambda^\mu(p_A)\bar{u}_\nu^{(s_1)}(k_1)\gamma^\mu(g - g'\gamma_5)v_\nu^{(s_2)}(k_2)\bar{v}_\nu^{(s_2)}(k_2)(g + g'\gamma_5)\gamma^\nu u_\nu^{(s_1)}(k_1)\varepsilon_\lambda^{*\nu}(p_A) \tag{3.10}$$

Since the polarization ε commutes with the other elements, the completeness relation for massive vector bosons

$$\sum_\lambda \varepsilon_\lambda^\mu(p_A)\varepsilon_\lambda^{*\nu}(p_B) = -g^{\mu\nu} + \frac{p_A^\mu p_B^\nu}{M_{Z'}^2}. \tag{3.11}$$

27

elements can be applied. Note that here $g^{\mu\nu}$ is the Minkowski metric (see equation elements2.47) and not the coupling constant. Using this relation the expression becomes:

$$|\mathcal{M}|^2 = \bar{u}_\nu^{(\mathrm{s}_1)}(k_1)\Big(-g^{\mu\nu} + \frac{p_\mathrm{A}^\mu p_\mathrm{A}^\nu}{M_{Z'}^2}\Big)\gamma^\mu(g - g'\gamma_5)v_\nu^{(\mathrm{s}_2)}(k_2)\bar{v}_\nu^{(\mathrm{s}_2)}(k_2)(g + g'\gamma_5)\gamma^\nu u_\nu^{(\mathrm{s}_1)}(k_1). \quad (3.12)$$

As mentioned in section 2.6.1, it is necessary to sum over the different spins of the neutrino and antineutrino and average over the possible initial polarizations of Z' (see equation 2.57). For simplicity, only one component will be considered, allowing every part of the term to commute. Applying these considerations, the invariant amplitude becomes:

$$
\begin{aligned}
|\overline{\mathcal{M}}|^2 &= \frac{1}{3}\Big(-g^{\mu\nu} + \frac{p_\mathrm{A}^\mu p_\mathrm{A}^\nu}{M_{Z'}^2}\Big)\bar{u}_\nu^{(\mathrm{s}_1)}(k_1)_\mathrm{a}\big[\gamma^\mu(g - g'\gamma_5)\big]_{\mathrm{ab}}v_\nu^{(\mathrm{s}_2)}(k_2)_\mathrm{b}\bar{v}_\nu^{(\mathrm{s}_2)}(k_2)_\mathrm{c}\big[(g + g'\gamma_5)\gamma^\nu\big]_{\mathrm{cd}}u_\nu^{(\mathrm{s}_1)}(k_1)_\mathrm{d} \\
&= \frac{1}{3}\Big(-g^{\mu\nu} + \frac{p_\mathrm{A}^\mu p_\mathrm{A}^\nu}{M_{Z'}^2}\Big)u_\nu^{(\mathrm{s}_1)}(k_1)_\mathrm{d}\bar{u}_\nu^{(\mathrm{s}_1)}(k_1)_\mathrm{a}\big[\gamma^\mu(g - g'\gamma_5)\big]_{\mathrm{ab}}v_\nu^{(\mathrm{s}_2)}(k_2)_\mathrm{b}\bar{v}_\nu^{(\mathrm{s}_2)}(k_2)_\mathrm{c}\big[(g + g'\gamma_5)\gamma^\nu\big]_{\mathrm{cd}}
\end{aligned}
$$
$$(3.13)$$

Recall that the Einstein summation convention also includes Latin indices. After rearranging and since the spin sum is applied, the relations

$$\sum_s u^{(s)}(p)_\mathrm{a}\bar{u}^{(s)}(p)_\mathrm{b} = (\slashed{p} + m)_{\mathrm{ab}}, \quad (3.14)$$

$$\sum_s v^{(s)}(p)_\mathrm{a}\bar{v}^{(s)}(p)_\mathrm{b} = (\slashed{p} - m)_{\mathrm{ab}}, \quad (3.15)$$

as well as the Feynman slash notation $\slashed{p} \equiv \gamma^\mu p_\mu$ are used. Plugging this into the expression 3.13 gives

$$|\overline{\mathcal{M}}|^2 = \frac{1}{3}\Big(-g^{\mu\nu} + \frac{p_\mathrm{A}^\mu p_\mathrm{A}^\nu}{M_{Z'}^2}\Big)\mathrm{Tr}\big[(\slashed{k}_1 + m_\nu)\gamma^\mu(g - g'\gamma_5)(\slashed{k}_2 - m_\nu)(g + g'\gamma_5)\gamma^\nu\big]. \quad (3.16)$$

In this thesis the neutrinos are approximated to be massless, so the term becomes:

$$|\overline{\mathcal{M}}|^2 = \frac{1}{3}\Big(-g^{\mu\nu} + \frac{p_\mathrm{A}^\mu p_\mathrm{A}^\nu}{M_{Z'}^2}\Big)\mathrm{Tr}\big[\slashed{k}_1\gamma^\mu(g - g'\gamma_5)\slashed{k}_2(g + g'\gamma_5)\gamma^\nu\big] \quad (3.17)$$

$$= \frac{1}{3}\Big(-g^{\mu\nu} + \frac{p_\mathrm{A}^\mu p_\mathrm{A}^\nu}{M_{Z'}^2}\Big)\mathrm{Tr}\big[\slashed{k}_1\gamma^\mu\slashed{k}_2(g + g'\gamma_5)^2\gamma^\nu\big] \quad (3.18)$$

$$= \frac{1}{3}\Big(-g^{\mu\nu} + \frac{p_\mathrm{A}^\mu p_\mathrm{A}^\nu}{M_{Z'}^2}\Big)\mathrm{Tr}\big[\slashed{k}_1\gamma^\mu\slashed{k}_2(g^2 + g'^2 + 2g'\gamma_5)\gamma^\nu\big]. \quad (3.19)$$

The trace of an odd number of γ-matrices vanishes, so only terms containing an even number are considered. For the trace of γ-matrices, the identities in appendix A are utilized. In the expression 3.19 for the invariant amplitude the trace with the γ_5-matrix vanishes because k_1 and k_2 are symmetric under permutation and the epsilon-Tensor in

those indices is not. So the expression gets

$$|\overline{\mathcal{M}}|^2 = \frac{1}{3}\left(-g^{\mu\nu} + \frac{p_A^\mu p_A^\nu}{M_{Z'}^2}\right)(g^2 + g'^2)k_1^\sigma k_2^\rho \text{Tr}\left[\gamma^\sigma \gamma^\mu \gamma^\rho \gamma^\nu\right] \tag{3.20}$$

$$= \frac{1}{3}(g^2 + g'^2)k_1^\sigma k_2^\rho\left(-g^{\mu\nu} + \frac{p_A^\mu p_A^\nu}{M_{Z'}^2}\right)\text{Tr}\left[\gamma^\sigma \gamma^\mu \gamma^\rho \gamma^\nu\right] \tag{3.21}$$

$$= \frac{1}{3}(g^2 + g'^2)k_1^\sigma k_2^\rho\left(8g^{\rho\sigma} + \frac{8p_A^\rho p_A^\sigma}{M_{Z'}^2} - \frac{4p_A^2 g^{\rho\sigma}}{M_{Z'}^2}\right) \tag{3.22}$$

$$= \frac{1}{3}(g^2 + g'^2)\left(8(k_1k_2) + \frac{8(p_A k_1)(p_A k_2) - 4p_A^2(k_1k_2)}{M_{Z'}^2}\right). \tag{3.23}$$

Plugging in the results of the scalar products

$$p_A^2 = E_A = M_{Z'} \tag{3.24}$$

$$k_1k_2 = \begin{pmatrix} E_\nu \\ \vec{k_1} \end{pmatrix}\begin{pmatrix} E_\nu \\ -\vec{k_1} \end{pmatrix} = E_\nu^2 + \vec{k_1}^2 = E_\nu^2 + E_\nu^2 - m_\nu = 2E_\nu^2 = \frac{1}{2}M_{Z'}^2 \tag{3.25}$$

$$p_A k_i = \begin{pmatrix} E_A \\ 0 \end{pmatrix}\begin{pmatrix} E_\nu \\ \vec{k_i} \end{pmatrix} = E_A E_\nu = M_{Z'}\frac{1}{2}M_{Z'} = \frac{1}{2}M_{Z'}^2 \tag{3.26}$$

gives:

$$|\overline{\mathcal{M}}|^2 = \frac{1}{3}\frac{(g^2 + g'^2)}{M_{Z'}^2}\left(4M_{Z'}^2 + 2M_{Z'}^2 - 2M_{Z'}^2\right) \tag{3.27}$$

$$= \frac{1}{3}4(g^2 + g'^2)M_{Z'}^2. \tag{3.28}$$

One last step needs to be done. Because there are three different generations of neutrinos this result needs to be multiplied by three, resulting in

$$|\overline{\mathcal{M}}|^2 = 4(g^2 + g'^2)M_{Z'}^2, \tag{3.29}$$

as the final expression of the invariant amplitude. With equation 2.58 the decay width of the $Z \to \nu\bar{\nu}$-decay concludes to be

$$\Gamma_{Z'\to\nu\nu} = \frac{|\vec{k_1}|}{32\pi^2 M_{Z'}^2}\int 4(g^2 + g'^2)M_{Z'}^2 d\Omega \tag{3.30}$$

$$= \frac{|\vec{k_1}|}{32\pi^2 M_{Z'}^2}4(g^2 + g'^2)M_{Z'}^2\int d\Omega \tag{3.31}$$

$$= \frac{|\vec{k_1}|}{32\pi^2 M_{Z'}^2}4(g^2 + g'^2)M_{Z'}^2 4\pi \tag{3.32}$$

$$= \frac{|\vec{k_1}|(g^2 + g'^2)}{2\pi} \tag{3.33}$$

The absolute of the momentum can be rewritten as

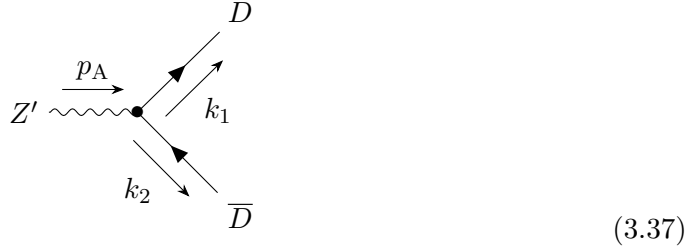$$E_\nu^2 = m_\nu^2 |\vec{k_1}|^2 \tag{3.34}$$

$$\Leftrightarrow \qquad |\vec{k_1}| = \sqrt{E_\nu^2 - m_\nu^2} = \sqrt{\frac{1}{4}M_{Z'}^2} = \frac{1}{2}M_{Z'} \tag{3.35}$$

giving the expression

$$\boxed{\Gamma_{Z'\to\nu\bar\nu} = \frac{(g^2 + g'^2)}{4\pi}M_{Z'}} \tag{3.36}$$

as the decay width for this first decay.

The Feynman diagram for the second decay is

$$\tag{3.37}$$

Analog to the previous decay the chain and its hermitian adjoint conclude to be

$$\mathcal{M} = \varepsilon_\lambda^\mu(p_A)\bar{u}_D^{(s_1)}(k_1)ig_X\gamma^\mu(1-\gamma_5)v_D^{(s_2)}(k_2)$$
$$= i\varepsilon_\lambda^\mu(p_A)g_X\bar{u}_D^{(s_1)}(k_1)\gamma^\mu(1-\gamma_5)v_D^{(s_2)}(k_2) \tag{3.38}$$
$$\mathcal{M}^\dagger = -v_D^{\dagger(s_2)}(k_2)(1-\gamma_5)^\dagger\gamma^{\nu\dagger}u_D^{\dagger(s_1)}(k_1)g_X^\dagger\varepsilon_\lambda^{*\nu}(p_A)i$$
$$= -i\varepsilon_\lambda^{*\nu}(p_A)g_X\bar{v}_D^{(s_2)}(k_2)(1+\gamma_5)\gamma^\nu u_D^{(s_1)}(k_1) \tag{3.39}$$

So for the amount square the result is

$$|\mathcal{M}|^2 = \left(-g^{\mu\nu}+\frac{p_A^\mu p_A^\nu}{M_{Z'}^2}\right)g_X^2\bar{u}_D^{(s_1)}(k_1)\gamma^\mu(1-\gamma_5)v_D^{(s_2)}(k_2)\bar{v}_D^{(s_2)}(k_2)(1+\gamma_5)\gamma^\nu u_D^{(s_1)}(k_1). \tag{3.40}$$

Only regarding one component, making use of the relations 3.14 and 3.15, and using the trace identities the invariant amplitude becomes

$$|\overline{\mathcal{M}}|^2 = \frac{2}{3}g_X^2 k_2^\sigma k_1^\rho\left(8g^{\rho\sigma} + \frac{8p_A^\rho p_A^\sigma}{M_{Z'}^2} - \frac{4p_A^2 g^{\rho\sigma}}{M_{Z'}^2}\right). \tag{3.41}$$

The scalar products result in

$$p_A^2 = E_A = M_{Z'} \tag{3.42}$$

$$k_1 k_2 = \begin{pmatrix} E_\nu \\ \vec{k_1} \end{pmatrix} \begin{pmatrix} E_\nu \\ -\vec{k_1} \end{pmatrix} = E_\nu^2 + \vec{k_1}^2 = E_\nu^2 + E_\nu^2 - m_D^2 = 2E_\nu^2 - m_D^2 = \frac{1}{2}M_{Z'}^2 - m_D^2 \tag{3.43}$$

$$p_A k_i = \begin{pmatrix} E_A \\ 0 \end{pmatrix} \begin{pmatrix} E_\nu \\ \vec{k_i} \end{pmatrix} = E_A E_\nu = M_{Z'} \frac{1}{2} M_{Z'} = \frac{1}{2}M_{Z'}^2. \tag{3.44}$$

Plugging this results and the additional factor 3 into the invariant amplitude gives

$$|\overline{\mathcal{M}}|^2 = \frac{8}{3}g_X^2(M_{Z'}^2 - m_D^2) \tag{3.45}$$

and with equation 2.58 the decay width for the second decay is

$$\boxed{\Gamma_{Z' \to D\overline{D}} = \frac{g_X^2}{6\pi}M_{Z'}\sqrt{1 - \frac{4m_D^2}{M_{Z'}^2}}\left(1 - \frac{m_D^2}{M_{Z'}^2}\right)} \tag{3.46}$$

The total decay width for the vector portal Z' is the addition of the two decay widths calculated above:

$$\Gamma_{Z'} = \Gamma_{Z' \to \nu\overline{\nu}} + \Gamma_{Z' \to D\overline{D}}. \tag{3.47}$$

3.2.2 Annihilation of $D\bar{D}$ into $\nu\bar{\nu}$

The first annihilation process happens when the DM particle collides with its antiparticle and they produce a pair of neutrino and antineutrino through the Z'-portal as interaction boson. The Feynman diagram for this process is

$$\tag{3.48}$$
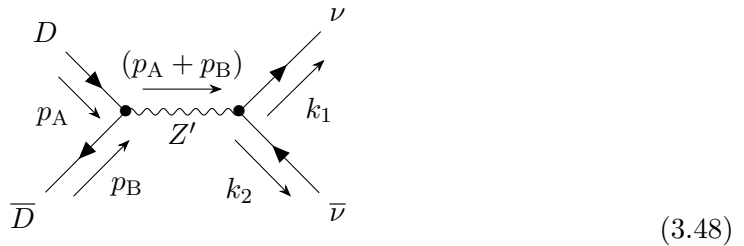
Because the propagator has the momentum $q \equiv (p_A + p_B) = \sqrt{s}$, this process is referred to as the *s-channel*. In this scenario, it is the only channel that occurs. This contrasts with the other annihilation process, where the *t-* and *u-channels* are involved. Again,

the different parts of the diagram lead to the chain

$$\mathcal{M} = \left[\bar{v}_\mathrm{D}^{(s_1)}(p_\mathrm{B}) i g_\mathrm{X} \gamma^\mu (1 - \gamma_5) u_\mathrm{D}^{(s_2)}(p_\mathrm{A}) \right] \frac{-i \left(g^{\mu\nu} - \frac{q^\mu q^\nu}{M_{Z'}^2} \right)}{q^2 - M_{Z'}^2} \left[\bar{u}_\nu^{(s_3)}(k_1) i \gamma^\nu (g - g' \gamma_5) v_\nu^{(s_4)}(k_2) \right]$$

$$= -i g_\mathrm{X} \frac{\left(-g^{\mu\nu} + \frac{q^\mu q^\nu}{M_{Z'}^2} \right)}{q^2 - M_{Z'}^2} \left[\bar{v}_\mathrm{D}^{(s_1)}(p_\mathrm{B}) \gamma^\mu (1 - \gamma_5) u_\mathrm{D}^{(s_2)}(p_\mathrm{A}) \right] \left[\bar{u}_\nu^{(s_3)}(k_1) \gamma^\nu (g - g' \gamma_5) v_\nu^{(s_4)}(k_2) \right]$$

(3.49)

Notice that the Z' boson has a different term than in the decays. This is because here it acts as a propagator and not as an incoming particle. The hermitian adjoint of the chain is

$$\mathcal{M}^\dagger = i g_\mathrm{X} \frac{\left(-g^{\sigma\rho} + \frac{q^\rho q^\sigma}{M_{Z'}^2} \right)}{q^2 - M_{Z'}^2} \left[\bar{v}_\nu^{(s_4)}(k_2)(g + g' \gamma_5) \gamma^\sigma u_\nu^{(s_3)}(k_1) \right] \left[\bar{u}_\mathrm{D}^{(s_2)}(p_\mathrm{A})(1 + \gamma_5) \gamma^\rho v_\mathrm{D}^{(s_1)}(p_\mathrm{B}) \right].$$

(3.50)

Multiplying $\mathcal{M}$ and $\mathcal{M}^\dagger$ results in

$$|\mathcal{M}|^2 = g_\mathrm{X}^2 \frac{\left(-g^{\mu\nu} + \frac{q^\mu q^\nu}{M_{Z'}^2} \right) \left(-g^{\sigma\rho} + \frac{q^\rho q^\sigma}{M_{Z'}^2} \right)}{(q^2 - M_{Z'}^2)^2} \left[\bar{v}_\mathrm{D}^{(s_1)}(p_\mathrm{B}) \gamma^\mu (1 - \gamma_5) u_\mathrm{D}^{(s_2)}(p_\mathrm{A}) \right]$$

$$\left[\bar{u}_\nu^{(s_3)}(k_1) \gamma^\nu (g - g' \gamma_5) v_\nu^{(s_4)}(k_2) \right] \left[\bar{v}_\nu^{(s_4)}(k_2)(g + g' \gamma_5) \gamma^\sigma u_\nu^{(s_3)}(k_1) \right]$$

$$\left[\bar{u}_\mathrm{D}^{(s_2)}(p_\mathrm{A})(1 + \gamma_5) \gamma^\rho v_\mathrm{D}^{(s_1)}(p_\mathrm{B}) \right]$$

(3.51)

With the temporary substitution for better oversight

$$F^{\mu\nu\rho\sigma} = g_\mathrm{X}^2 \frac{\left(-g^{\mu\nu} + \frac{q^\mu q^\nu}{M_{Z'}^2} \right) \left(-g^{\sigma\rho} + \frac{q^\rho q^\sigma}{M_{Z'}^2} \right)}{(q^2 - M_{Z'}^2)^2},$$

(3.52)

and summing over the spins of the outgoing neutrinos and averaging over the spins of the incoming DM particles while regarding only one component and making use of the fermion spin sum relations (3.14 and 3.15) the invariant amplitude for this annihilation is

$$|\overline{\mathcal{M}}|^2 = \frac{1}{4} F^{\mu\nu\rho\sigma} \mathrm{Tr} \left[(p\!\!\!/_B - \mathrm{m}_\mathrm{D}) \gamma^\mu (1 - \gamma_5)(p\!\!\!/_A + \mathrm{m}_\mathrm{D})(1 + \gamma_5) \gamma^\rho \right]$$

$$\mathrm{Tr} \left[k\!\!\!/_1 \gamma^\nu (g - g' \gamma_5) k\!\!\!/_2 (g + g' \gamma_5) \gamma^\sigma \right].$$

(3.53)

Note that $q^2 = s$. With the trace identities and calculating the scalar products including $F^{\mu\nu\rho\sigma}$

$$|\overline{\mathcal{M}}|^2 = \frac{12 g_\mathrm{X}^2}{(s - M_{Z'}^2)^2} \left[(g^2 + g'^2) \left(s^2 + 2st - 2 m_\mathrm{D}^2 s + 2 \left(m_\mathrm{D}^2 - t \right)^2 \right) + 2sgg' \left(2t + s - 2m_\mathrm{D}^2 \right) \right]$$

(3.54)

32

is the result for the invariant amplitude of this first annihilation. Note that here again the additional factor 3 was added, because of the three neutrino generations. To obtain the total cross section the integral 2.64 needs to be performed. This results in

$$\sigma'_{\mathrm{D}\bar{\mathrm{D}}\to\nu\bar{\nu}} = \frac{g_{\mathrm{X}}^2(g^2 + g'^2)}{2\pi} \frac{\sqrt{s}(s - m_{\mathrm{D}}^2)}{\sqrt{s - 4m_{\mathrm{D}}^2}(s - M_{Z'}^2)^2} \tag{3.55}$$

as the cross section for this process. To prevent that the cross section tends to infinity at the resonance $M_{Z'} = 2m_{\mathrm{D}}$ the total decay width needs to be included in the denominator, because in this case the Z' boson is created on shell and can decay through the processes calculated before. So the final cross section for $D\bar{D} \to \nu\bar{\nu}$ is

$$\boxed{\sigma_{\mathrm{D}\bar{\mathrm{D}}\to\nu\bar{\nu}} = \frac{g_{\mathrm{X}}^2(g^2 + g'^2)}{2\pi} \frac{\sqrt{s}\left(s - m_{\mathrm{D}}^2\right)}{\sqrt{s - 4m_{\mathrm{D}}^2}\left[(s - M_{Z'}^2)^2 + M_{Z'}^2\Gamma_{Z'}^2\right]}.} \tag{3.56}$$

3.2.3 Annihilation of $D\bar{D}$ into $Z'Z'$

As previously mentioned, this process involves both *t-* and *u-channel*. This means that the matrix element is the sum of the matrix elements of both channels $\mathcal{M} = \mathcal{M}_{\mathrm{t}} + \mathcal{M}_{\mathrm{t}}$. So for the total invariant amplitude of this process

$$|\overline{\mathcal{M}}|^2 = |\overline{\mathcal{M}_{\mathrm{t}}}|^2 + |\overline{\mathcal{M}_{\mathrm{u}}}|^2 + 2\mathrm{Re}(\mathcal{M}_{\mathrm{t}}\mathcal{M}_{\mathrm{u}}^\dagger) \tag{3.57}$$

needs to be calculated.

t-channel

For the *t-channel* of this annihilation the Feynman diagram looks like this:

$$\tag{3.58}$$
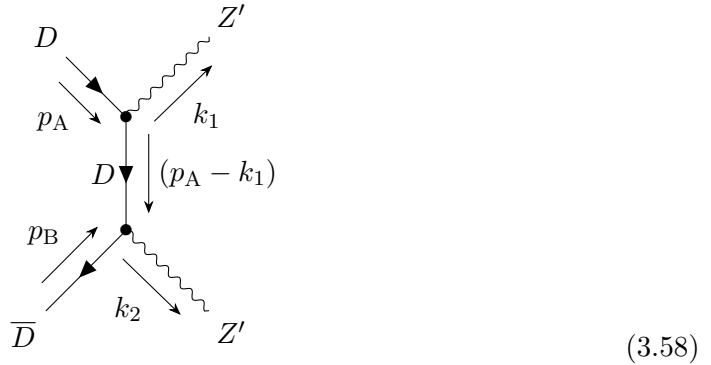
See how here the momentum of the propagator, which is D in this case, is $(p_A - k_1) = t \equiv q_t^2$. So applying the according rules the chain

$$
\begin{aligned}
\mathcal{M}_t &= \left[\bar{v}_D^{(s_1)}(p_B) i g_X \gamma^\mu (1 - \gamma_5) \frac{i(\slashed{q}_t + m_D)}{q_t^2 - m_D^2} i g_X \gamma^\nu (1 - \gamma_5) u_D^{(s_2)}(p_A) \right] \varepsilon_{\lambda_1}^{*\nu}(k_1) \varepsilon_{\lambda_2}^{*\mu}(k_2) \\
&= \frac{-2 i g_X^2}{t - m_D^2} \varepsilon_{\lambda_1}^{*\nu}(k_1) \varepsilon_{\lambda_2}^{*\mu}(k_2) \left[\bar{v}_D^{(s_1)}(p_B) \gamma^\mu \slashed{q}_t (1 + \gamma_5) \gamma^\nu u_D^{(s_2)}(p_A) \right],
\end{aligned} \tag{3.59}
$$

and the adjoint

$$
\mathcal{M}_t^\dagger = \frac{2 i g_X^2}{t - m_D^2} \varepsilon_{\lambda_1}^{\sigma}(k_1) \varepsilon_{\lambda_2}^{\rho}(k_2) \left[\bar{u}_D^{(s_2)}(p_A) \gamma^\sigma (1 - \gamma_5) \slashed{q}_t \gamma^\rho v_D^{(s_1)}(p_B) \right] \tag{3.60}
$$

can be obtained. Multiplying these and following the same steps as in chapter 3.2.2 results in

$$
\begin{aligned}
|\mathcal{M}_t|^2 = \frac{1}{4} \frac{8 g_X^4}{(t - m_D^2)^2} \Bigg\{ &-\frac{2}{M_{Z'}^4} \Big[4 M_{Z'}^8 - 4 M_{Z'}^6 \left(m_D^2 + 2t \right) + M_{Z'}^4 \left(t(4s + 5t) - 3 m_D^4 \right) \\
&+ 2 M_{Z'}^2 \left(m_D^2 - t \right) \left(m_D^4 - 2 m_D^2 t + t(2s + t) \right) + \left(m_D^2 - t \right)^2 \left(m_D^4 - 2 m_D^2 t + t(s + t) \right) \Big] \Bigg\}
\end{aligned} \tag{3.61}
$$

for the amount square of the *t-channel*. An additional factor $\frac{1}{2}$ is necessary, because the two outgoing Z'-bosons are indistinguishable:

$$
\begin{aligned}
|\overline{\mathcal{M}_t}|^2 = \frac{g_X^4}{(t - m_D^2)^2} \Bigg\{ &-\frac{2}{M_{Z'}^4} \Big[4 M_{Z'}^8 - 4 M_{Z'}^6 \left(m_D^2 + 2t \right) + M_{Z'}^4 \left(t(4s + 5t) - 3 m_D^4 \right) \\
&+ 2 M_{Z'}^2 \left(m_D^2 - t \right) \left(m_D^4 - 2 m_D^2 t + t(2s + t) \right) + \left(m_D^2 - t \right)^2 \left(m_D^4 - 2 m_D^2 t + t(s + t) \right) \Big] \Bigg\}
\end{aligned} \tag{3.62}
$$

This gives the first part to calculate the invariant amplitude with equation 3.57.

u-channel

Here the Feynman diagram looks like this:

$$(3.63)$$
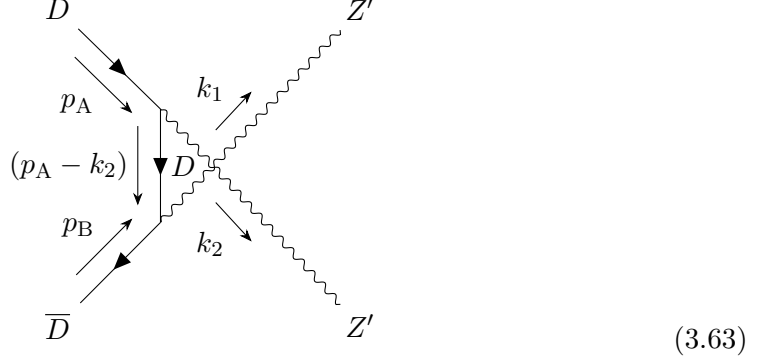
Analog to the *t-channel* the results

$$\mathcal{M}_u = \frac{-2ig_X^2}{u - m_D^2} \varepsilon_{\lambda_1}^{*\nu}(k_1) \varepsilon_{\lambda_2}^{*\mu}(k_2) \left[\bar{v}_D^{(s_1)}(p_B) \gamma^\nu q\!\!\!/_u (1 + \gamma_5) \gamma^\mu u_D^{(s_2)}(p_A) \right] \tag{3.64}$$

$$\mathcal{M}_u^\dagger = \frac{2ig_X^4}{u - m_D^2} \varepsilon_{\lambda_1}^\sigma(k_1) \varepsilon_{\lambda_2}^\rho(k_2) \left[\bar{u}_D^{(s_2)}(p_A) \gamma^\rho q\!\!\!/_u (1 + \gamma_5) \gamma^\sigma v_D^{(s_1)}(p_B) \right] \tag{3.65}$$

$$\Rightarrow |\overline{\mathcal{M}_u}|^2 = \frac{g_X^4}{(u - m_D^2)^2} \left\{ -\frac{2}{M_{Z'}^4} \left[8M_{Z'}^8 + 4M_{Z'}^6 \left(7m_D^2 - 5(s + t) \right) \right. \right.$$

$$+ M_{Z'}^4 \left(29m_D^4 - 44m_D^2(s + t) + 17(s + t)^2 \right) + 2M_{Z'}^2 \left(-m_D^2 + s + t \right)^2$$

$$\left. \left. \left(3m_D^2 - 2s - 3t \right) + \left(-m_D^2 + s + t \right)^2 \left(m_D^4 - 2m_D^2 t + t(s + t) \right) \right] \right\} \tag{3.66}$$

can be derived. With the previous result from the *t-channel* the interference term is

$$2\mathrm{Re}\left[\mathcal{M}_t \mathcal{M}_u^\dagger \right] = \frac{2g_X^4}{(t - m_D^2)(u - m_D^2)} \left\{ -\frac{2}{M_{Z'}^4} \left[M_{Z'}^6 \left(8m_D^2 - 2(4s + t) \right) \right. \right.$$

$$+ M_{Z'}^4 \left(-9m_D^4 + 2m_D^2(6s - t) + t(9s + 5t) \right) - 4M_{Z'}^2(s + t) \left(m_D^4 - 2m_D^2 t + t(s + t) \right)$$

$$\left. \left. + \left(m_D^4 - 2m_D^2 t + t(s + t) \right)^2 \right] \right\}. \tag{3.67}$$

So this

$$
|\overline{\mathcal{M}}|^2 = -\frac{4g_{\mathrm{X}}^4}{M_{Z'}^4 \left(m_{\mathrm{D}}^2 - t\right)^2 \left(-2M_{Z'}^2 - m_{\mathrm{D}}^2 + s + t\right)^2} \Bigg\{
$$

$$
2M_{Z'}^8 \left[-12m_{\mathrm{D}}^4 + 10m_{\mathrm{D}}^2 s + s^2 + 6st + 14t^2\right]
$$

$$
+ 2M_{Z'}^6 \left[10m_{\mathrm{D}}^6 - 4m_{\mathrm{D}}^4(s + 5t) + m_{\mathrm{D}}^2\left(-5s^2 + 10st + 18t^2\right) - 2t(s + 2t)^2\right]
$$

$$
+ 8M_{Z'}^{12} - 8M_{Z'}^{10}(s + 3t) + M_{Z'}^4 \left[28m_{\mathrm{D}}^8 - 4m_{\mathrm{D}}^6(9s + 20t) + m_{\mathrm{D}}^4\left(19s^2 + 80st + 80t^2\right)\right.
$$

$$
\left. - 4m_{\mathrm{D}}^2 t\left(6s^2 + 13st + 8t^2\right) + 2t(s + t)\left(s^2 + 2st + 2t^2\right)\right] - m_{\mathrm{D}}^2 s\left(m_{\mathrm{D}}^2 - t\right)\left(m_{\mathrm{D}}^2 - s - t\right)
$$

$$
\left(m_{\mathrm{D}}^4 - 2m_{\mathrm{D}}^2 t + t(s + t)\right) + 2M_{Z'}^2 m_{\mathrm{D}}^2 \left(m_{\mathrm{D}}^2 - t\right)\left[2m_{\mathrm{D}}^6 - 2m_{\mathrm{D}}^4(2s + 3t) + \right.
$$

$$
\left. 2m_{\mathrm{D}}^2\left(s^2 + 5st + 3t^2\right) - (s + t)\left(s^2 + 4st + 2t^2\right)\right]\Bigg\} \tag{3.68}
$$

is the expression for the invariant amplitude that will be used to calculate the cross section, with equation 2.64, for the $D\bar{D} \to Z'Z'$ process. The cross section concludes to be

$$
\sigma_{\mathrm{D}\overline{\mathrm{D}}\to \mathrm{Z'Z'}} = \frac{g_{\mathrm{X}}^4}{4\pi M_{Z'}^4 s\left(s - 4m_{\mathrm{D}}^2\right)}\Bigg\{\frac{\sqrt{\left(s - 4M_{Z'}^2\right)\left(s - 4m_{\mathrm{D}}^2\right)}}{M_{Z'}^4 + m_{\mathrm{D}}^2(s - 4M_{Z'}^2)}
$$

$$
\left(m_{\mathrm{D}}^4(s - 8M_{Z'}^2 s + 14M_{Z'}^4) + m_{\mathrm{D}}^2(24M_{Z'}^6 - 7M_{Z'}^4 s) - 8M_{Z'}^8\right)
$$

$$
\frac{2\left[m_{\mathrm{D}}^4(6M_{Z'}^4 + 4M_{Z'}^2 s - s^2) + 2M_{Z'}^4(s^2 + 4M_{Z'}^4) + 2M_{Z'}^2 m_{\mathrm{D}}^2(s^2 - 6M_{Z'}^2 s - 8M_{Z'}^4)\right]}{s - 2M_{Z'}^2}\ln B\Bigg\},
$$

with

$$
B = \frac{s - 2M_{Z'}^2 + \sqrt{(s - 4M_{Z'}^2)(s - 4m_{\mathrm{D}}^2)}}{s - 2M_{Z'}^2 - \sqrt{(s - 4M_{Z'}^2)(s - 4m_{\mathrm{D}}^2)}}. \tag{3.69}
$$

With the sum of the cross sections of the two processes

$$
\sigma = \sigma_{\mathrm{D}\overline{\mathrm{D}}\to\nu\bar{\nu}} + \sigma_{\mathrm{D}\overline{\mathrm{D}}\to\mathrm{Z'Z'}} \tag{3.70}
$$

the total annihilation cross section from the hidden sector is calculated.

3.2.4   Non-relativistic thermal averages

Following the steps in section 2.6.3 the s-wave contribution for the two annihilation processes can be derived, to later set constrains on the parameters of the DM model in section 3.3.2. If the mass of the DM particle is smaller than the mass of the interaction bososn, the annihilation into neutrinos will be the dominant at FO and the final relic

density is determined by the $D\bar{D} \to \nu\bar{\nu}$ process. With the presented procedure

$$a = \frac{3m_D^2 g_X^2 (g^2 + g'^2)}{\pi(M_{Z'}^2 - 4m_D^2)^2} \tag{3.71}$$

is the term for the *s-wave*-contribution of the first annihilation process. If m_D is greater than $M_{Z'}$ the $D\bar{D} \to Z'Z'$ process becomes kinematically accessible and will play a greater roll in determining the final relic density. Here

$$a' = \frac{g_X^4 m_D^2}{\pi M_{Z'}^2 (2m_D^2 - M_{Z'}^2)}\left(1 - \frac{M_{Z'}^2}{m_D^2}\right)^{3/2} \tag{3.72}$$

is the derived term for the *s-wave* contribution of the second annihilation process.

3.3 Numerical Calculation

In this section the numerical solution to solve the Boltzmann equation is presented. The calculation was fully implemented in MATLAB, and the plots and the constraints were created and calculated using Python. The most important scripts are appended in appendix D. For the results the mass ratio $R = M_{Z'}/m_D$ is used instead of the mass of the portal. At first the expressions for the cross sections 3.56 and 3.69 are transferred into the Script `Oh2Calculator`, in which the ODE is solved with `ode15s` [24] and Ωh^2 is calculated. It uses the function `SigmaV22` to calculate the thermally averaged cross section according to equation 2.72. With the yield in equilibrium 2.42, everything to solve the Boltzmann equation for the yield 2.41 is given. This is done in the lines:

```
47  %% ODE Solver
48  options = odeset ( 'RelTol',1e-5,'AbsTol',1e-100 );
49  tspan = [xstart xend];
50  initialCondition = Y_eq(tspan(1,1));
51
52  [x, Y] = ode15s(@(x, Y) Boltzmann_rhs(x, Y), tspan,
        initialCondition, options);
```

The initial condition to solve the differential equation is chosen as $Y(x_{start}) = Y_{eq}(x_{start})$, because for high temperatures the DM decoupling did not take place and the DM is still in equilibrium. After solving the ODE the first time, the freeze-out point x_{FO} is determined, as the point where the ratio of the $Y(x)$ and $Y_{eq}(x)$ is greater than 2.5. This Value is now used as `xend` for the `ode15s`. With the yield at the decoupling Y_{FO} and the freeze out temperature, `IntergateTillToday` uses equation 2.43 to approximate the resulting Yield for today, which is than used in equation 2.44 to finally calculate the resulting relic density `Oh2`.

The parameters to vary are m_D, R, g_X, g, and g' resulting in a five dimensional parameter space. To grasp the impact the parameters have on the final relic density for all further

calculations g' is set equal to g, lowering the dimensions of the parameter space from five to four. The results are stored in a text file to plot them in Python.

3.3.1 Grid Scans

By constructing for-loops around `Oh2calculator` it is possible to do grid scans over two Parameters, while the other two are fixed and observe how Ωh^2 changes depending on the two variables.

Furthermore the grid scans in this section were made with a resolution of $200 \times 200 = 40000$ data points

Grid Scan $m_{\mathrm{D}} - R$

The fist grid scan is over R and m_{D} with

$$
\begin{aligned}
&0.5 < R < 4, && \text{in linear steps} \\
&10^1 < m_{\mathrm{D}} < 10^3, && \text{in logarithmic steps} \\
&g = 0.1 \\
&g_{\mathrm{X}} = 0.2
\end{aligned}
$$

and is presented in the heat-map 3.1, where the colour represents the relic density calculated. The regions where the correct final relic density ($\Omega h^2 = 0.12 \pm 0.01$) is achieved are marked in pink. For Values $R \rightarrow 2$ there is a anomaly noticeable. The code struggles to compute the calculation with the resulting white areas showing in the figure. This white areas have no physical implication.

To start analyzing the result and set it into physical context the general impact of m_{D} on Ωh^2 can be observed. No matter what R is, the relic density is proportional to m_{D}. It can be traced to the connection between cross sections and the relic density. If the cross section is high, the DM particles annihilate more often, leading to a lower abundance of DM at FO and hence a lower final relic density. If m_{D} increases, the annihilations get kinematically more difficult, and the cross section decreases resulting in an increase of the final relic density. So the code describes this behaviour correctly.

Also interesting is the dependency on R. The two Values $R = 1$ and $R = 2$ seem important, because the tendency of Ωh^2 changes here. For $R < 1$ the process $D\bar{D} \rightarrow Z'Z'$ is kinematically accessible and therefore dominant at FO and determines the final relic density and for $R \rightarrow 1$ the cross section decreases, because the Z'-Portal gets heavier (regarding one fixed m_{D}). This happens until at $R = 1$ the annihilation into Z' gets kinematically excluded. So for $R > 1$ the annihilation $D\bar{D} \rightarrow \nu\bar{\nu}$ sets the final relic density. If the ratio increases more, this means that the Z'-Portal gets heavier than the DM-fermion, which leads to a preferred Annihilation into neutrinos lowering the number of DM at FO.

For $R = 2$ a resonance occurs, which leads to a drastic drop of the final relic density. In this case Z' is exactly twice as heavy as the Portal enabling the $Z' \rightarrow D\bar{D}$ decay. In the
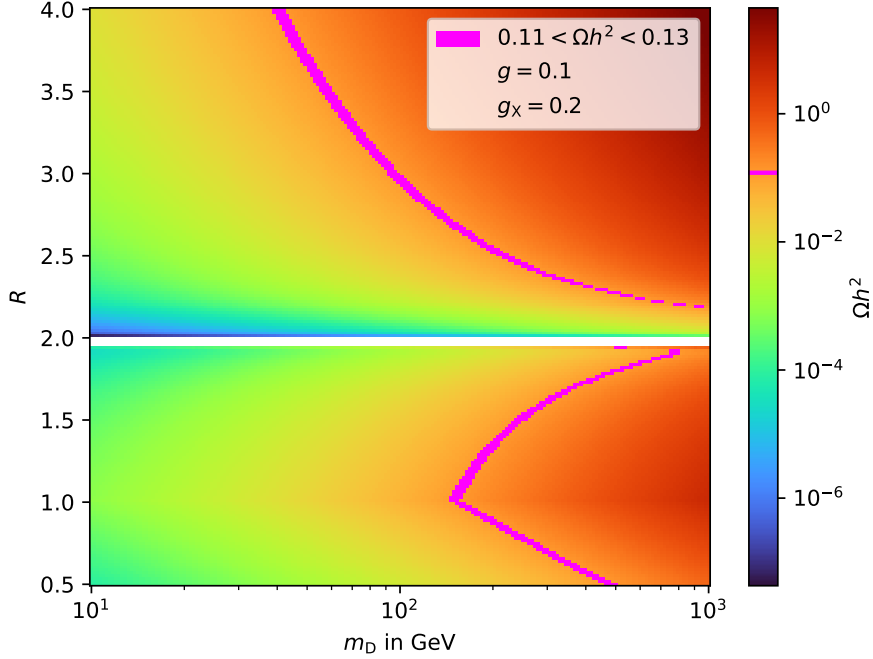
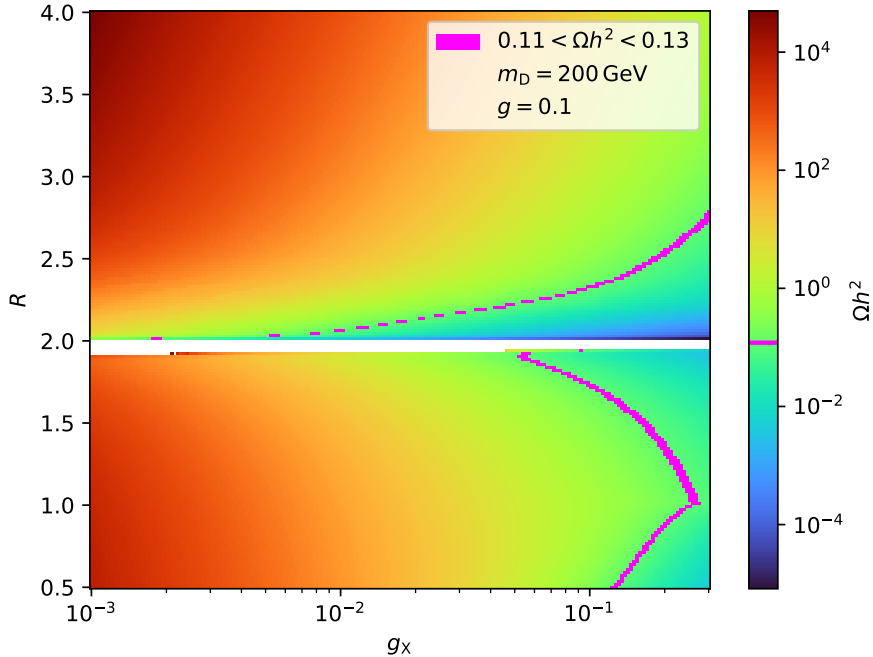Figure 3.1: Ωh^2 for the grid scan of m_D and R. The relic density is represented in the colour in a logarithmic scale. The pink area represents those combination that give $\Omega h^2 = 0.12 \pm 0.01$. The fixed parameters are $g = 0.1$ and $g_X = 0.2$. For $R \to 2$ (the resonance) the code struggles explaining the white areas.

Code this resonance is not simulated well, because instead of giving results that tend to zero it returns exactly zero or negative densities (more in section 4).

Once the mass of the portal is greater than than twice the DM mass the cross section just gets smaller and smaller for higher R, leading to a steady increasing of Ωh^2. This tendency does seem to flatten out, but should continue for $R \to \infty$.

Grid Scan $g_X - R$

This grid scan is over the parameters g_X and R with

$$0.5 < R < 4, \qquad \text{in linear steps}$$
$$10^{-3} < g_X < 0.3, \qquad \text{in logarithmic steps}$$
$$g = 0.1$$
$$m_D = 100\,\text{GeV}$$

The result is presented in figure 3.2 Since an increment of the coupling g_X affects both Processes and increases the cross section, it has the opposite effect than an increment of m_D resulting in a mirrored behaviour of the final relic density along the x-axis. The dependency of R does not change and is analogous to **Grid Scan $m_D - R$**

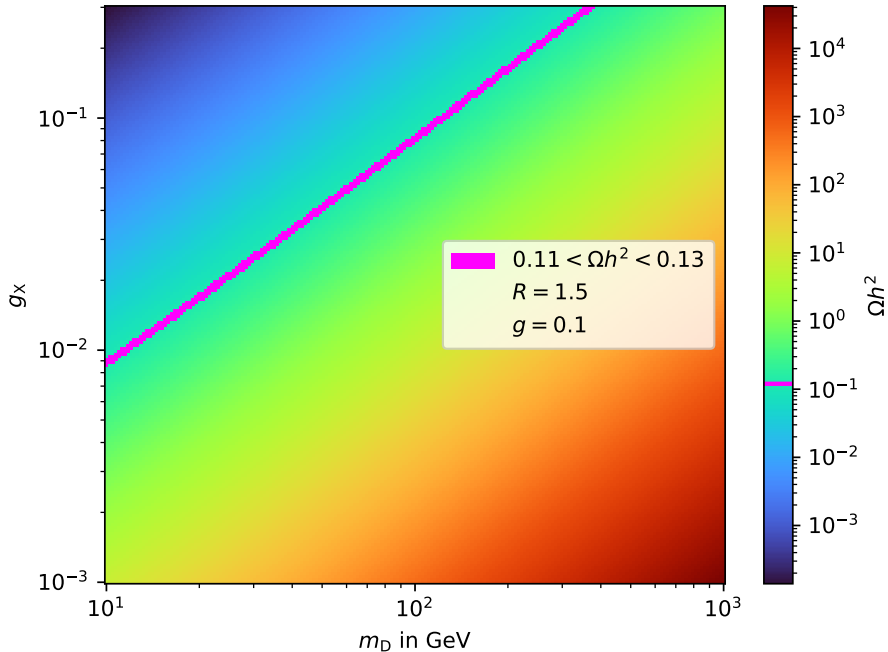Figure 3.2: Ωh^2 for the grid scan of g_X and R. The relic density is represented in the colour in a logarithmic scale. The pink area represents those combination that give $\Omega h^2 = 0.12 \pm 0.01$. The fixed parameters are $g = 0.1$ and $m_D = 100\,\text{GeV}$. For $R \to 2$ (the resonance) the code fails and returns nonphysical results.

Grid Scan $m_D - g_X$

As the last example the grid scan over m_D and g_X is shown in figure 3.3, with the parameters

$$0.5 < m_D < 4, \qquad \text{in logarithmic steps}$$
$$10^{-3} < g_X < 0.3, \qquad \text{in logarithmic steps}$$
$$R = 1.5$$
$$g = 0.1$$

Here the resonance is not visible, because R is set to 1.5 and does not change. The connection between the parameters m_D and g_x and the final relic density were mentioned earlier. For higher masses the cross section decreases and the relic density at FO increases. For increasing couplings it is vice versa and the final Ωh^2 decreases. This matches the depiction in figure 3.3.

To control the accuracy of the results a comparison to `micrOMEGAs` is made in appendix C. `micrOMEGAs` is a code used for the calculation of DM properties including the relic density for generic models. The deviation to the results of `micrOMEGAs` are generally under 10%, but obviously it diverges for values approaching the resonance at $R = 2$. Also for the value of $R = 1$ a small discrepancy can be observed, indicating that the switch of one process to another does not compute smoothly. Nevertheless for the $m_D - g_X$ grid

Figure 3.3: Ωh^2 for the grid scan of m_D and g_X. The relic density is represented in the colour in a logarithmic scale. The pink area represents those combination that give $\Omega h^2 = 0.12 \pm 0.01$. The fixed parameters are $R = 1.5$ and $g = 0.1$.

scan the maximal percentage deviation is below 4%, showing that the code produces good results across the rest of the parameter space.

3.3.2 Indirect Detection Constraint

The DM particle in this model only annihilates into neutrinos. So the experiments around the world that measure the neutrino flux constrains the parameter space of this model. In [25] the restrictions on the first factor of the expansion by existing and future experiments are elaborated. Using the data of that paper the restriction of the first order of $\langle \sigma v \rangle_{\text{n.r}} = a$ is shown in figure 3.4. Only the experiments that cover the range used in this thesis are taken into account and to express the results in natural units the conversion $1\,\text{cm}^3\text{s}^{-1} = 8.57 \cdot 10^{16}\,\text{GeV}^{-2}$ is used. To determine the parameter space excluded, for each combination of the parameters, The expression for the *s-wave* contributions 3.71 and 3.72 from section 3.2.4 are compared to the upper limit given by the (future) experiments. If the expansion factor is larger, this combination is excluded as a possibility. Doing this for the $m_D - R$ grid scan the excluded areas in the parameter space are added in figure 3.5.
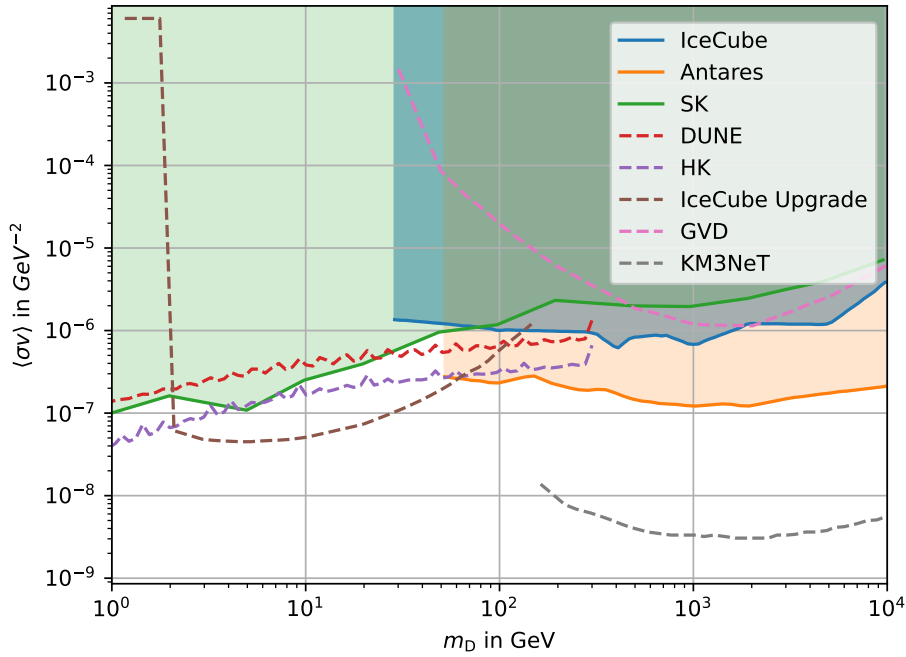
Figure 3.4: Using the data of [25] the restriction on the first expansion factor depending on m_D are obtained. With the expression from section 3.2 the parameter space of this model can be constrained.
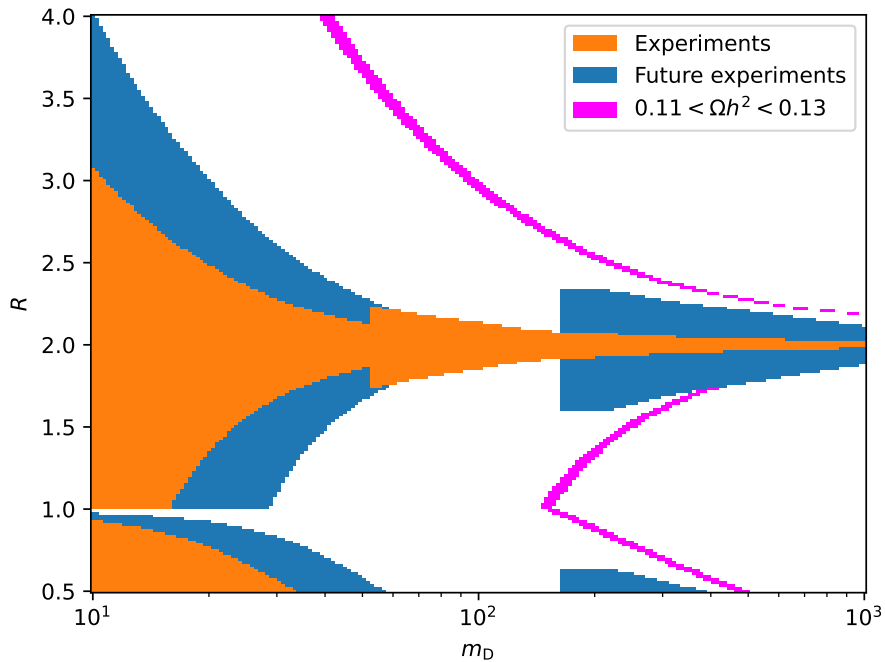
Figure 3.5: The constrains from the neutrino experiments are added to the grid scan of 3.1. The constraints imposed by the requirement for the correct relic density are stricter than the restrictions set by existing experiments
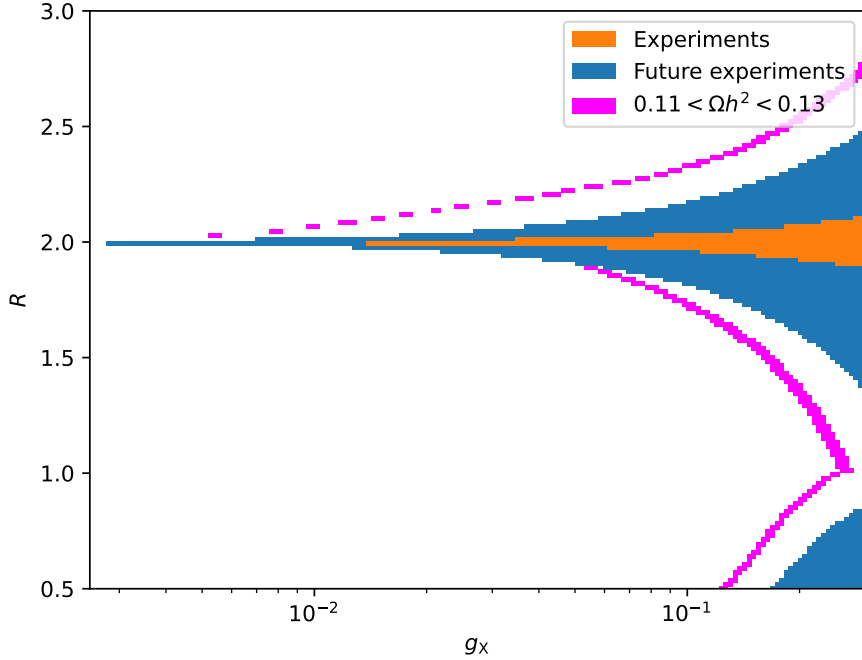
Figure 3.6: Constrains for the $g_X - R$ grid scan. Here neither the already existing nor the future experiments set significant constrains, so that the strictest restriction comes from the correct relic density.

It can be observed that the existing experiments do not constrain the model strictly enough to exclude some combinations that give the correct result. However, future experiments are expected to examine a small section of the parameter space that results in the correct relic density. Having a look at figure 3.4 it is obvious that the strictest constraints for m_D values over $200\,\mathrm{GeV}$ in the future will come from the *KM3NeT* experiment.[6] Also the failing of the code at the resonance is not very problematic, since this area is almost completely excluded. The same procedure is done for the other grid scans resulting in the added exclusion areas in figures 3.6 and 3.7. In 3.6 the excluded area of the experiments does not restrict the combinations that lead to the correct final relic density and the future experiments only constrain a small portion at the resonance. For the $m_D - g_X$ scan the constrains are not strict enough to give an relevant limitation of the parameter space that yields in the correct final density (see figure 3.7).

The conclusion is that either the existing nor the future planned experiment set constrains strict enough to verify the parameters of this model that conclude in the correct value for Ωh^2. Only some small areas are excluded by the future experiment *KM3NeT*.

---

[6]KM3NeT is a future underwater neutrino telescope experiment located in the Mediterranean Sea, designed to explore distant astrophysical sources and study neutrino properties using optical sensors [26].
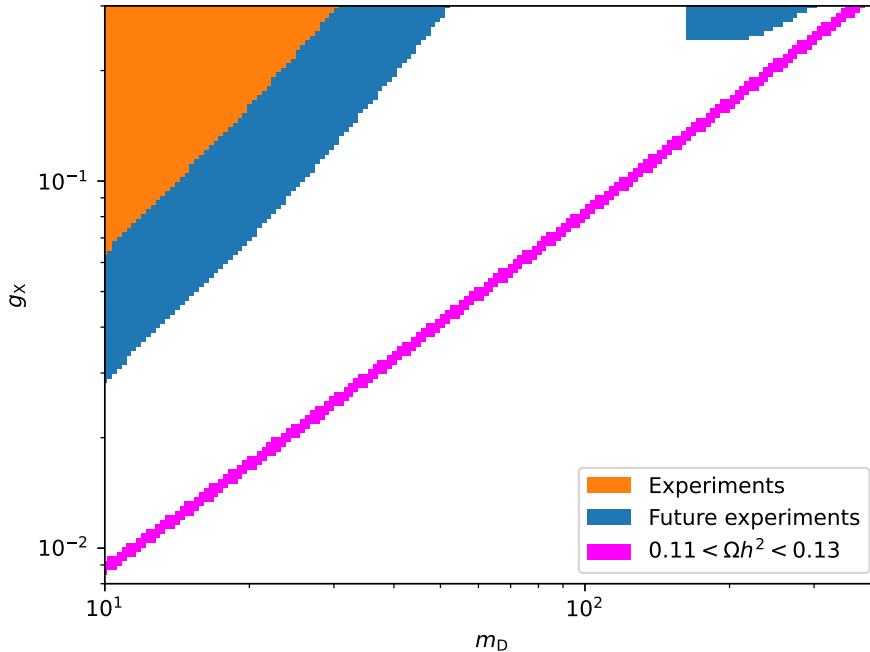
Figure 3.7: Constrains for the $m_D - g_X$ grid scan. Here again the correct relic density sets the stricter limitations to the parameter space than the restrictions coming from either the already existing nor the future experiments

3.3.3 Parameter Optimizing with the Bisection Method

Regarding the proportion of the combinations that give the correct relic density ($\Omega h^2 = 0.12 \pm 0.01$) to the combinations that lead to wrong results, it is obvious that most of the computing time is used to calculate unnecessary combinations. To consider only relevant combinations a bisection method is used to find the corresponding parameter that concludes in the correct relic density for a fixed combination of the other parameters. The function `optimizeParameter.m` does exactly this using `Oh2calculator.m` to calculate Ωh^2 in each iteration. `optimizeParameter.m` takes the parameter to optimize as a string and returns the optimized value of it, ensuring the relic density is the expected result. Some changes were made to the typical structure of a bisection method. Instead of using a tolerance for the bisected parameter[7] a tolerance for the resulting Ωh^2 is implemented. Also because it is difficult to predict the range in which the optimal parameter lies, a stuck counter is initialized to interrupt the loop if the bisection results 15 consecutive times in a value within one percent of the lower or upper bound. The output value is then the last set value.

In `OptimizeGridSearch.m` for-loops are build around the optimize function in a similar way as in `GridSearch.m`. So now it is possible to find combinations of three parameters

---

[7]Normally a tolerance is set to determine the accuracy of the bisected parameter, i.e. the method keeps working while (upper_limit - lower_limit > tolerance).

that conclude in the correct relic density and not just two as in the method of the plain grid scan. The accuracy of the following scans is set to 0.01, meaning for all combinations the final relic density is $\Omega h^2 = 0.12 \pm 0.01$ (except the bisection method gets stuck on the lower or upper limit), showing how the parameter need to change to get the correct relic density. The grid scans have a total data points of 50×50, reducing the resolution from 40000 to 2500.

Optimize m_D for $g_X - R$
In this scan the optimal value for m_D is determined for this set of parameters:

$$0.5 < R < 4, \qquad\qquad \text{in linear steps}$$
$$10^{-3} < g_X < 0.3, \qquad\qquad \text{in logarithmic steps}$$
$$g = 0.1$$

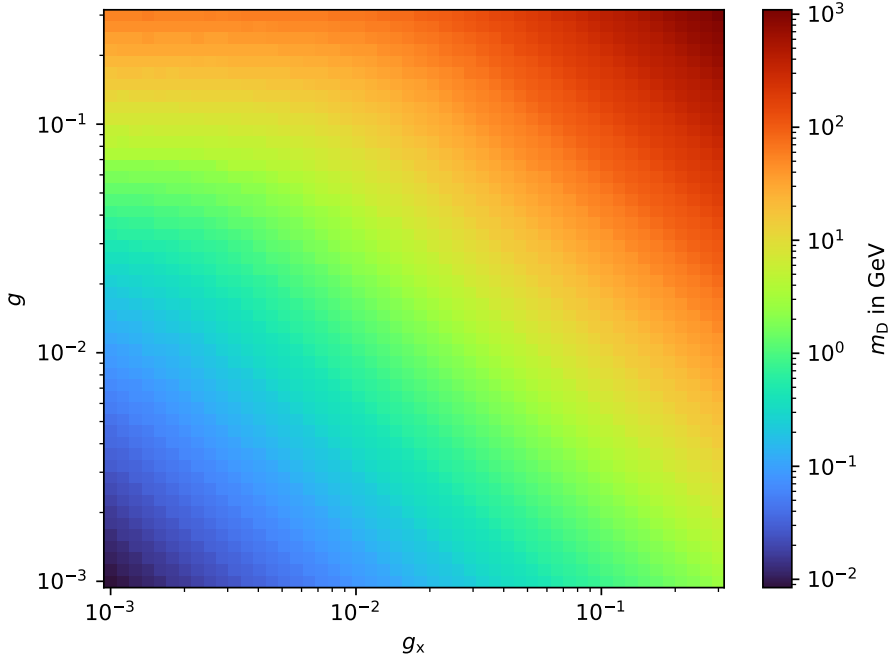This is depicted in figure 3.8.
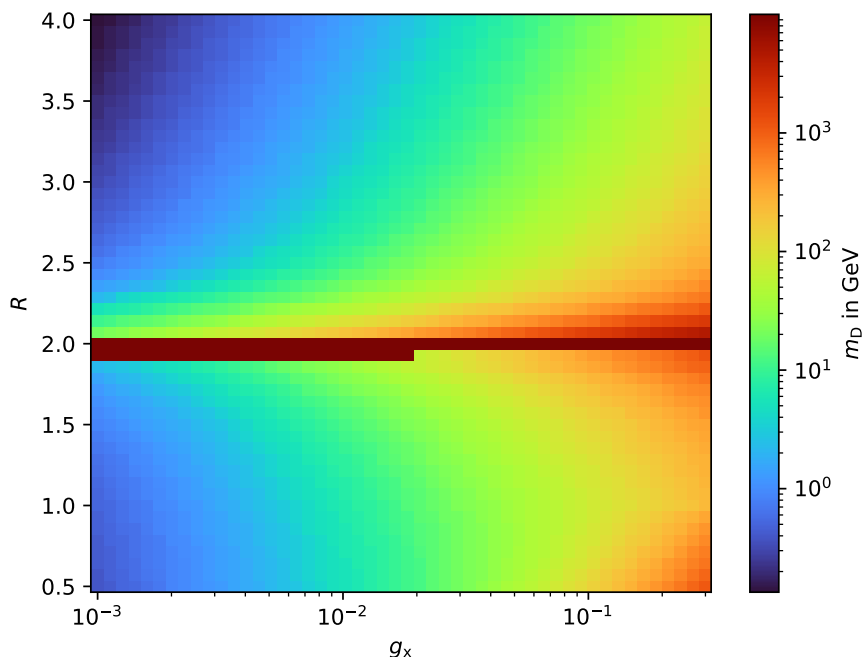
Figure 3.8: Optimal m_D for the grid scan of g_X and R. For each combination of these parameters the calculated relic density is $\Omega h^2 = 0.12 \pm 0.01$. The fixed parameter is $g = 0.1$.

As a fist step to interpret the heat map the way m_D has to change when g_X increases to still hit the targeted density. For every R an increment of g_X leads to a increment of the mass. This makes sense, because a greater g_X result in a lower Ωh^2 and to counter this effect, the mass has to increase. At the resonance m_D theoretically has to tend to infinity, to compensate the relic density, which tends to zero.

Optimize m_D for $g_\mathrm{X} - g$

As another example for optimization of a parameter by the bisection method m_D is optimized for different couplings g_X and g. The chosen parameters are:

$$10^{-3} < g_\mathrm{X} < 0.3, \qquad \text{in logarithmic steps}$$
$$10^{-3} < g < 0.3, \qquad \text{in logarithmic steps}$$
$$R = 1.5$$

The result is shown in figure 3.9.

Figure 3.9: Optimal m_D for the grid scan of g_X and g. For each combination of these parameters the calculated relic density is $\Omega h^2 = 0.12 \pm 0.01$. The fixed parameter is $R = 1.5$.

The influence of the couplings on the cross section is known. In general the increment of a coupling increases the cross section and therefore decreases the final relic density. For g this is only the case for ratios over one, because else the process determining Ωh^2 is $D\bar{D} \to \nu\bar{\nu}$, which does not depend on g. The results of the grid scan indicate that either for higher g or g_X the relic density drops, which leads to a necessary increment of the DM mass, to encounter this effect. Besides it is noticeable that for high g and low g_X ($g > 7 \times 10^{-2}$ and $g_\mathrm{X} < 5 \times 10^{-3}$) a change of the coupling to the dark sector does not have any impact on m_D, meaning that is does not have a impact on the final relic density. This makes sense, because in the dominant process g_X and g appear once (in the first order of the Feynman diagram) and a increment of one would cancel out a decrease of the other. On the other hand this would mean that for high g_X and low

g the same tendency should be observable, which is not the case in this grid scan. A possible reason for the asymmetric appearance is that the couplings influence the relic density not in the same way and the effect would be visible for even higher g_X and lower g than the here used range.

4 Conclusion and Outlook

In this thesis a neutrinophilic dark matter model with a vector portal was investigated presented in section 3.1. With the given Lagrangians the possible interaction of the added hidden sector

- The $Z' \to \nu\bar{\nu}$ decay

- The $Z' \to D\bar{D}$ decay

- The $D\bar{D} \to \nu\bar{\nu}$ annihilation

- And the $D\bar{D} \to Z'Z'$ annihilation

were obtained. With the Feynman diagrams and the according rules, the decay width of the portal and the cross sections of the annihilation processes were calculated in section 3.2. These results were then implemented in *MATLAB* to numerically solve the Boltzmann equation for the yield. The effects of the four dimensional parameter space consisting of m_D, $M_\mathrm{Z'}$ (R as the mass ratio in the numerical calculations), g_X, and g was analyzed by doing grid scans over two parameters, while fixing the other two and observing how the final relic density changes for changes of the two scan parameters in section 3.3.1. The results show, that the final relic density increases with higher masses of the DM particle and decreases with higher coupling constants, as expected. Interesting is the dependency on the mass ratio R. Here the influence is not as linear as in the other parameters, because the dominant annihilation determines the final relic density and said changes if the mass of the vector portal is equal to the mass of the DM particle, leading to a complex behaviour. Additionally a resonance occurs at $R = 2$ in which the cross section gets big and the relic density abundance drop. Here the code fails to give correct results, so an improvement of the numerical method to handle the resonance will provide better results for that area in the parameter space and give a better understanding about the behaviour of the model near the resonance.

The comparison with `micrOMEGAs` shows that, excluding the resonance region, the code produces results that are generally accurate, with deviations around 10% from those of `micrOMEGAs`. In the $m_\mathrm{D} - g_\mathrm{X}$ grid scan, the maximum deviation observed was even lower with ca. 4%.

Because in this model only couples to neutrinos the experiments that measure neutrino flux can be used to constrain the parameter space, by giving an upper limit for the non-relativistic thermal average. Including this restrictions and considering future experiments, that will measure neutrino flux the parameter space can be narrowed. The results in section 3.3.2 show what regions are excluded from the (future) experiments. In general, one can say that the strictest constraints result from the correct relic density. Only a small section for $m_\mathrm{D} > 200\,\mathrm{GeV}$ in the future experiment *KM3NeT* will set stricter restrictions. This indicates that said experiment will be the only one in the near future with the potential to play a significant role in the search for dark matter, as it

explores a small region of the correct relic density.

At the end a bisection method was implemented to optimize one parameter (here m_{D} was chosen) in such way that for a set of other fixed parameters the correct relic density is matched. By performing grid scans over two parameters now combinations of three parameters can be found that conclude in the right result, showing how the mass of the DM particle needs to adapt to a change of the other parameters.

There are several avenues for future work to build upon the results of this thesis. First the better numerical calculation for the resonance can give a deeper understanding of the model in this area. Also the range of the grid scans can be expanded leading to additional insights of the model, to maybe uncover unknown behaviour and amplifying the impact of the constraints. These are possible approaches to improve and extend the results of this thesis and analyze the model in a deeper way. Of course the obvious next step is to amplify the model or use a different one and see how the results change to keep studying the dark matter and get a better understanding.

Overall, this thesis sets a solid foundation for understanding this specific model and presents analytical methods that can be applied to other models, potentially advancing our exploration of the nature of dark matter.

Appendices

A   Dirac-Matrices and Trace identities

In this section a closer look to the Dirac γ-matrices and the Trace relations including these is made using [27]. To understand the Dirac matrices at first the Pauli matrices

$$\sigma^1 = \begin{pmatrix} 0 & 1 \\ 1 & 0 \end{pmatrix}, \quad \sigma^2 = \begin{pmatrix} 0 & -i \\ i & 0 \end{pmatrix} \quad \text{and} \quad \sigma^3 = \begin{pmatrix} 1 & 0 \\ 0 & -1 \end{pmatrix} \tag{A.1}$$

need to be addressed. These are used to represent spin operators for spin $1/2$ particles in quantum mechanic and fulfill the Pauli algebra

$$[\sigma^i, \sigma^j] = 2i\varepsilon^{ijk}\sigma^k, \tag{A.2}$$

with ε^{ijk} is the *Levi-Civita*-tensor. Using the Pauli matrices the Dirac matrices can be constructed in the following way:

$$\gamma^0 = \begin{pmatrix} 1 & 0 \\ 0 & -1 \end{pmatrix}, \quad \gamma^i = \begin{pmatrix} 0 & \sigma^i \\ -\sigma^i & 0 \end{pmatrix} \tag{A.3}$$

Some fundamental relations of the γ-matrices are:

$$(\gamma^0)^2 = 1 \tag{A.4}$$

$$(\gamma^i)^2 = -1 \tag{A.5}$$

$$(\gamma^\mu)^\dagger = \gamma^0 \gamma^\mu \gamma^0 \tag{A.6}$$

$$\{\gamma^i, \gamma^j\} = 2g^{ij} \tag{A.7}$$

$$\{\gamma^0, \gamma^i\} = 0 \tag{A.8}$$

$$\gamma^\mu \gamma_\mu = 4 \tag{A.9}$$

$$\gamma^\mu \gamma^\alpha \gamma_\mu = -2\gamma^\alpha \tag{A.10}$$

with g being the Minkowski metric, and $\{a, b\} = ab + ba$ being the anti commutator. Often an additional fifth matrix

$$\gamma^5 = \gamma^0 \gamma^1 \gamma^2 \gamma^3 \tag{A.11}$$

is defined, with the properties:

$$(\gamma^5)^\dagger = \gamma^5 \tag{A.12}$$

$$(\gamma^5)^2 = 1 \tag{A.13}$$

$$\{\gamma^5, \gamma^\mu\} = 0. \tag{A.14}$$

These matrices fulfill the following trace identities

1. The trace of an odd number of γ-matrices vanishes:

$$\text{Tr}(\gamma^{\mu_1}\gamma^{\mu_2}\dots\gamma^{\mu_{2n+1}}) = \text{Tr}(\gamma^{\mu_1}\gamma^{\mu_2}\dots\gamma^{\mu_{2n+1}}\gamma^5\gamma^5)$$

(moving γ^5 over each γ^{μ_i}) $\qquad = -\text{Tr}(\gamma^5\gamma^{\mu_1}\gamma^{\mu_2}\dots\gamma^{\mu_{2n+1}}\gamma^5)$

(cyclic property of trace) $\qquad = -\text{Tr}(\gamma^{\mu_1}\gamma^{\mu_2}\gamma^5\gamma^5)$

$$= 0 \qquad\qquad (A.15)$$

2. The trace of the identity matrix is equal to one:

$$\text{Tr}(1) = 4 \qquad\qquad (A.16)$$

3. the trace of two γ- matrices is 4 times the Minkowski metric:

$$\text{Tr}(\gamma^\mu\gamma^\nu) = \text{Tr}(2g^{\mu\nu} - \gamma^\nu\gamma^\mu) \overset{(2.)}{=} 8g^{\mu\nu} - \text{Tr}(\gamma^\nu\gamma^\mu) = 8g^{\mu\nu} - \text{Tr}(\gamma^\mu\gamma^\nu)$$

$$\Rightarrow 2\text{Tr}(\gamma^\mu\gamma^\nu) = 8g^{\mu\nu} \Rightarrow \text{Tr}(\gamma^\mu\gamma^\nu) = 4g^{\mu\nu} \qquad (A.17)$$

This also results in:

$$\text{Tr}(\not{a}\not{b}) = 4ab \qquad\qquad (A.18)$$

4. The trace of the fifth Dirac matrix is zero:

$$\text{Tr}(\gamma^5) = \text{Tr}(\gamma^0\gamma^5\gamma^0) = -\text{Tr}(\gamma^5)$$

$$\Rightarrow \text{Tr}(\gamma^5) = 0 \qquad\qquad (A.19)$$

5. The trace of four Dirac matrices follow the relation:

$$\text{Tr}(\gamma^\mu\gamma^\nu\gamma^\rho\gamma^\sigma) = 4(g^{\mu\nu}g^{\rho\sigma} - g^{\mu\rho}g^{\nu\sigma} + g^{\mu\sigma}g^{\nu\rho}) \qquad\qquad (A.20)$$

6. And the trace of four γ-matrices with a γ^5-matrix is:

$$\text{Tr}(\gamma^5\gamma^\mu\gamma^\nu\gamma^\rho\gamma^\sigma) = -4\mathrm{i}\varepsilon^{\mu\nu\rho\sigma}, \qquad\qquad (A.21)$$

which are necessary for the calculation of the invariant amplitude.

B Feynman rules

Here the Feynman rules and how to derive the matrix element from the Feynman diagram by using those is explained in more detail making use of [27].
The Dirac equation

$$(i\gamma^\mu \partial_\mu - m)\Psi = 0 \tag{B.1}$$

is used to describe how fermions behave via a wave function that fulfills the equation. Ψ is the Dirac spinor and can be separated into two two-component spinors as
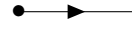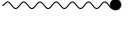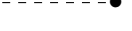
$$\Psi = \begin{pmatrix} \psi_1 \\ \psi_2 \end{pmatrix}, \tag{B.2}$$

where ψ_1 and ψ_2 are themselves two-component spinors. For free particle solutions, these can be interpreted as follows:

$$\Psi = \begin{pmatrix} u(p) \\ v(p) \end{pmatrix}, \tag{B.3}$$

where $u(p)$ is the spinor for fermions, which are particles with half-integer spin, positive energy, and moving forward in time, and $v(p)$ describes antifermions, which can be seen as particles with half-integer spin, positive energy, and moving backward in time. In the diagrams the difference between external and internal lines is made. External lines are represented by the polarization vector (in this thesis used for the decays of the Z' massive vector boson) or by the spinor (here the ingoing and outgoing fermions). The notation is visible in table B.1.

Table B.1: expressions for the different parts in a Feynman diagram to construct the chain (matrix element).[27]

particle	Feynman Rule	Depiction
ingoing fermion	$u(p)$	
outgoing fermion	$\bar{u}(p) = u^\dagger(p)\gamma^0$	
ingoing antifermion	$\bar{v}(p) = v^\dagger(p)\gamma^0$	
outgoing antifermion	$v(p)$	
ingoing vector boson	$\varepsilon^\mu(p)$	
outgoing vector boson	$\varepsilon^{*\mu}(p)$	
ingoing scalar boson	1	
outgoing scalar boson	1	

Here it gets visible that antifermions are treated as fermions moving back in time since in the Feynman diagrams the time is represented on the abscissa. Now for the particles that serve as propagator the Feynman rules differ. If a vector boson acts as propagator

the Feynman rules are:

$$\xrightarrow{q} \underset{m}{\sim\!\sim\!\sim} = -\frac{i\left(g^{\mu\nu - \frac{q^\mu q^\nu}{m^2}}\right)}{q^2 - m^2} \qquad \text{for massive bosons} \qquad (B.4)$$

$$\xrightarrow{q} \sim\!\sim\!\sim = -\frac{ig^{\mu\nu}}{q^2} \qquad \text{for massless bosons} \qquad (B.5)$$

Now if a fermion acts as prpagator

$$f \quad \bigg\downarrow q \quad = \frac{i(\slashed{q} + m)}{q^2 - m^2} \qquad (B.6)$$

is the according term to use in the chain. Also the spin sums (or completeness relations)

$$\sum_\lambda \varepsilon_\lambda^\mu(p_{\mathrm{A}})\varepsilon_\lambda^{*\nu}(p_{\mathrm{B}}) = -g^{\mu\nu} + \frac{p_{\mathrm{A}}^\mu p_{\mathrm{B}}^\nu}{m}. \qquad (B.7)$$

$$\sum_s u^{(s)}(p)_{\mathrm{a}}\bar{u}^{(s)}(p)_{\mathrm{b}} = (\slashed{p} + m)_{\mathrm{ab}} \qquad (B.8)$$

$$\sum_s v^{(s)}(p)_{\mathrm{a}}\bar{v}^{(s)}(p)_{\mathrm{b}} = (\slashed{p} - m)_{\mathrm{ab}}. \qquad (B.9)$$

used in the calculations are derived in [22]

C Comparison to `micrOMEGAs`

The comparison to the results of `microMEGAs` is presented in this Appendix.
`micrOMEGAs` is a code used for the calculation of DM properties including the relic density
for generic models. With a Python script it can be looped in the same way the grid scans
were made, so a comparison to the code used in this thesis is possible and a percentage
deviation can be analyzed to find the areas where differences occur. For the $m_{\mathrm{D}} - R$ grid
scan the deviation is depicted in figure C.1. The color scale is limited to a maximum
value of $100\,\%$, because at the resonance the discrepancy tends to infinity, which makes
it difficult to observe the deviation in the other regions.
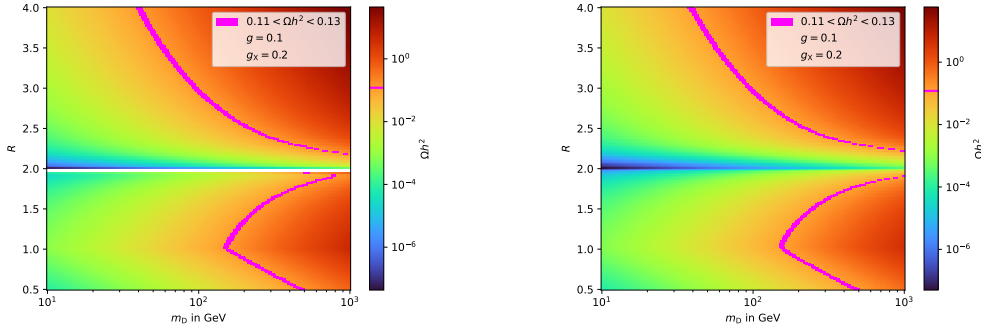
a) Previous result.

b) `micrOMEGAs` result.
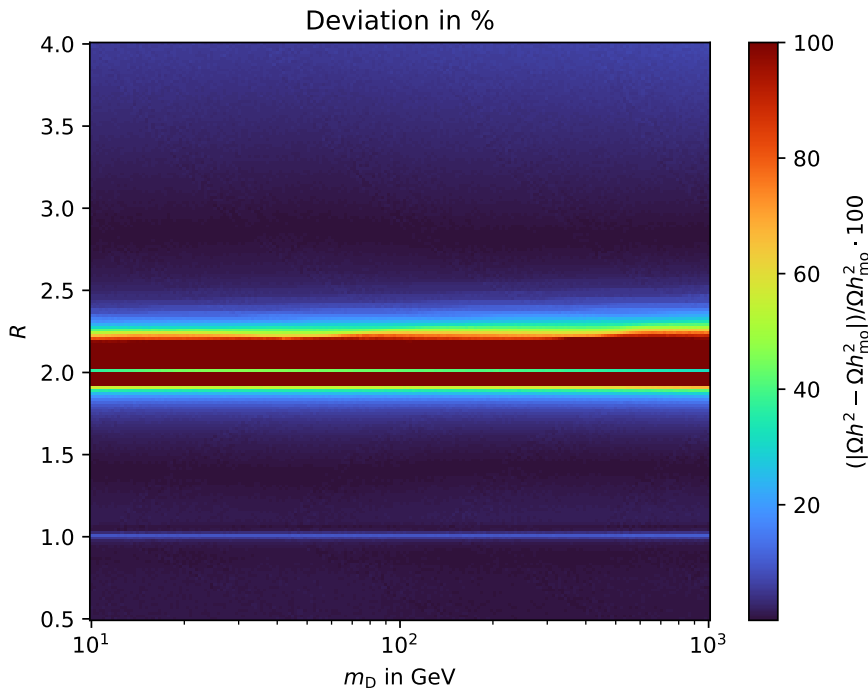
c) Percentage deviation of the relic density for m_D vs. R.

Figure C.1: Comparing both heat maps of the relic density it is obvious that the results of the two codes are similar. This is reflected in the deviation heat map. Except for the values approaching the resonance the discrepancy is about 10%. The mass of the DM particle seem to have no to little impact on the accuracy of the result.

As expected for values approaching the resonance the difference between the results gets greater. Apart of this both codes provide results that deviate from each other by less than 10%. Moreover, at $R = 1$, the discrepancy appears to be greater than for the ratios situated immediately above and below, which leads to the conclusion that the implementation of the change in the dominant process is distorting the relic density at this point. The value of m_D has almost no impact on the difference, leading to the conclusion that the calculation is correct over the span used for the mass of the DM

particle.

For the other two exemplar grids the comparison to `microOMEGAs` are shown in figure C.2 and C.3.

a) Previous result.

b) `microOMEGAs` result.

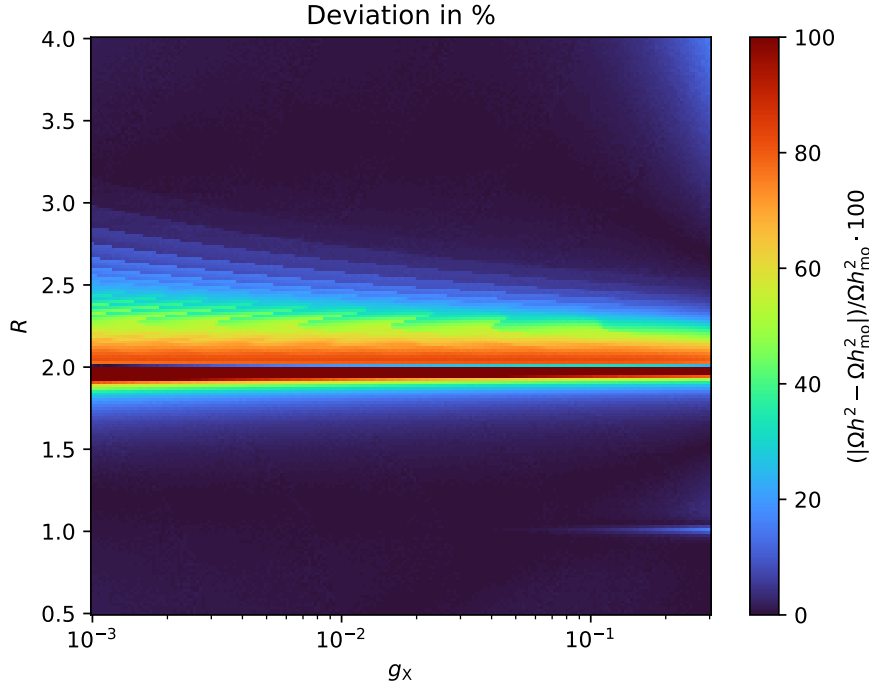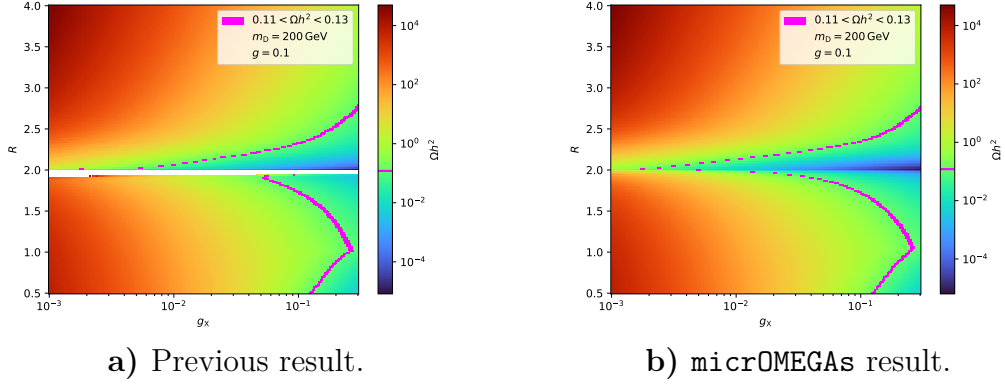**c)** Percentage deviation of the relic density for g_X vs R

Figure C.2: Here as well both code give similar results except for the resonance. For lower g_X the deviation increases.

Again as expected the deviation increases for ratios approaching the resonance. Also for lower couplings the deviation seem to increase, meaning that the code has trouble producing the correct result for this case.
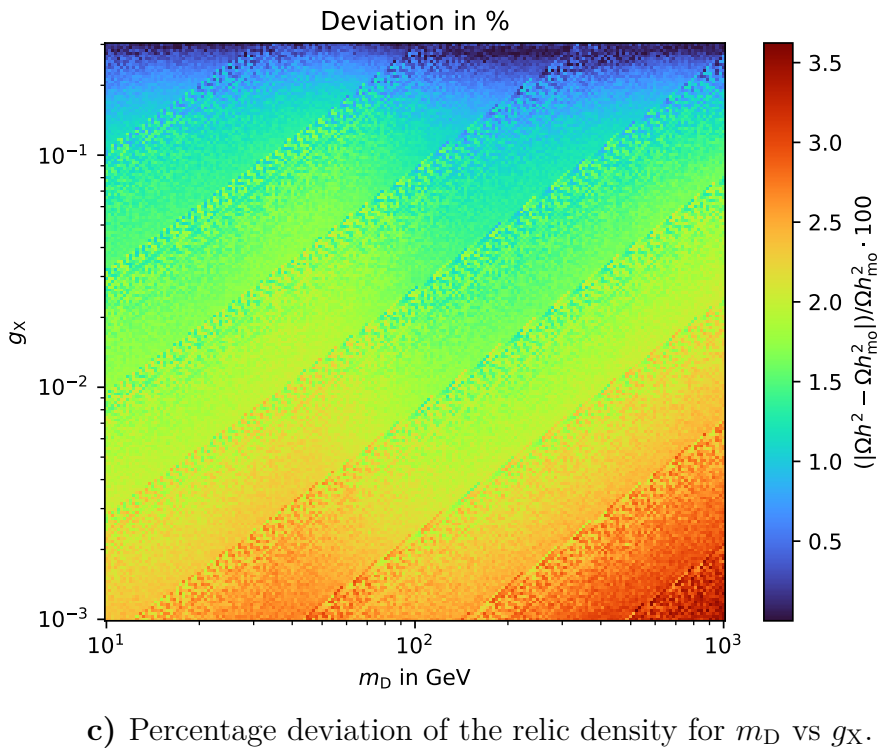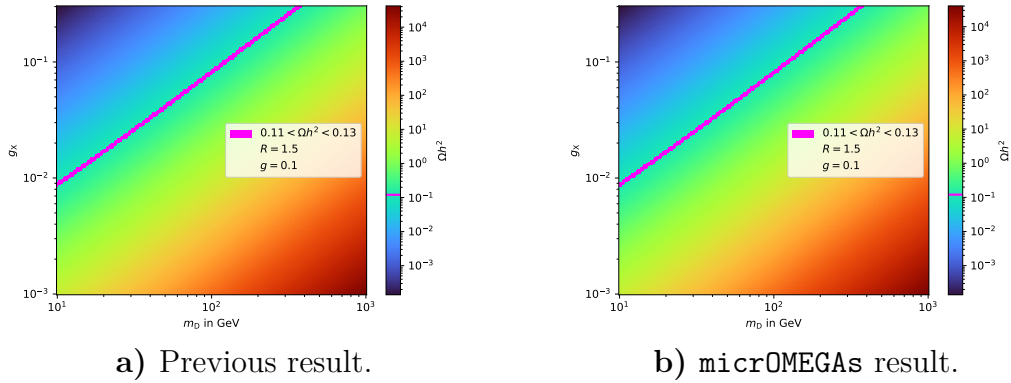
a) Previous result.

b) `micrOMEGAs` result.

c) Percentage deviation of the relic density for m_D vs g_X.

Figure C.3: For this grid scan the difference to `micrOMEGAs` for the whole range lies below 4 %.

Here the tendencies observed before are confirmed, because a change of m_D has a smaller impact than a reduction of g_X. This last comparison leads to the assumption that R is the parameter mainly responsible for the difference of the two codes, because for a fixed value the deviation does not fluctuate as much and it does not exceed a value of 4 %.

D   Code Scripts

Here some of the code used to calculate the results is presented:

Oh2Calculator.m

```matlab
format long e
% Add degrees of freedom
addpath bessel degrees_of_freedom
dof

%% Cross Sections
        DecayWidth_ZZnunu = (MZ * (g^2 + g_prime^2)) / (4 *
    pi);
        if R >= 2   % Z -> DD only if mZ >= 2mD, otherwise
    set width to zero
            DecayWidth_ZZDD = (gX^2 * MZ * (1 - mD^2 / MZ
    ^2) * sqrt(1 - 4 * mD^2 / MZ^2)) / (6 * pi);
        else
            DecayWidth_ZZDD = 0;
        end
        DecayWidth = DecayWidth_ZZDD + DecayWidth_ZZnunu;

        CrossSection_DDnunu = @(s) (gX^2 .* (g.^2 + g_prime
    .^2) .* sqrt(s) .* (s - mD.^2)) ./ (2 .* pi .* sqrt(s - 4 .*
     mD.^2) .* ((s - MZ.^2).^2 + MZ.^2 .* DecayWidth.^2));

        A = @(s) (gX.^4) ./ (4 .* pi .* MZ.^4 .* s .* (s -
    4 .* mD.^2));
        B = @(s) (sqrt((s - 4 .* MZ.^2) .* (s - 4 .* mD.^2)
    )) ./ (MZ.^4 + mD.^2 .* (s - 4 .* MZ.^2));
        C = @(s) mD.^4 .* (s.^2 - 8 .* MZ.^2 .* s + 14 .*
    MZ.^4) + mD.^2 .* MZ.^4 .* (24 .* MZ.^2 - 7 .* s) - 8 .* MZ
    .^8;
        D = @(s) (2 .* (mD.^4 .* (6 .* MZ.^4 + 4 .* MZ.^2
    .* s - s.^2) + 2 .* MZ.^4 .* (s.^2 + 4 .* MZ.^4) ...
                + 2 .* MZ.^2 .* mD.^2 .* (s.^2 - 6 .* MZ
    .^2 .* s - 8 .* MZ.^4))) ./ (s - 2 .* MZ.^2);
        E = @(s) (s - 2 .* MZ.^2 + sqrt((s - 4 .* mD.^2) .*
     (s - 4 .* MZ.^2))) ./ (s - 2 .* MZ.^2 - sqrt((s - 4 .* mD
    .^2) .* (s - 4 .* MZ.^2)));

        CrossSection_DDZZ = @(s) A(s) .* (B(s) .* C(s) + D(
```

```matlab
            s) .* log(E(s)));

            csSum = @(s) CrossSection_DDZZ(s) +
    CrossSection_DDnunu(s);

            % Cross sections at zero velocity
            csDDnunu_a = 3*mD^2*gX^2*(g^2+g_prime^2)/(pi*(MZ
    ^2-4*mD^2)^2);
            csDDnunu_b = gX^2*(g^2+g_prime^2)*mD^2*(MZ^2+20*mD
    ^2)/(4*pi*(MZ^2-4*mD^2)^3);

            csDDZZ_a   = gX^4*mD^2/(pi*MZ^2*(2*mD^2-MZ^2))*(1-
    MZ^2/mD^2)^(3/2);
            csDDZZ_b   = gX^4*sqrt(mD^2-MZ^2)/(24*pi*mD*MZ^4)
    *((32*mD^10-128*mD^8*MZ^2+272*mD^6*MZ^4 ...
                          -192*mD^4*MZ^6+45*mD^2*MZ^8+MZ^10)/(MZ
    ^2-2*mD^2)^4);

            %% Equilibrium Yield
            g_D = 2.0;
            Y_eq = @(x) (45.*g_D*x.^2.*besselk(2,x))./(4.*pi
    .^4.*heff(mD./x));

            %% Boltzmann Equation
            entropy          = @(T) (2.*pi.^2./45).*heff(T).*T
    .^3;

            Boltzmann_rhs    = @(x,Y) sqrt(90./(pi.^2.*geff(mD
    ./x))).*gtilde(mD./x).*x.*MPlanck./mD.^2.*(entropy(mD./x)
    ...
                                   .*(SigmaV22(mD./x, mD,
    mD, CrossSection_DDnunu)+SigmaV22(MZ./x, MZ, MZ,
    CrossSection_DDZZ)) ...
                                   .*(Y_eq(x).^2-Y.^2));

            %% ODE Solver
            options = odeset ( 'RelTol',1e-5,'AbsTol',1e-100 );
            tspan = [xstart xend];
            initialCondition = Y_eq(tspan(1,1));

            [x, Y] = ode15s(@(x, Y) Boltzmann_rhs(x, Y), tspan,
```

```matlab
    initialCondition, options);

        counter = 0;
        for i=1:length(x)
            y_ratio = Y(i)/Y_eq(x(i));
            if y_ratio >= 2.5
                xf = x(i);
                counter = counter + 1;
            end
            if counter == 1
                break
            end
        end

    tspan_new = [xstart xf];
    [x, Y]    = ode15s(@(x, Y) Boltzmann_rhs(x, Y),
tspan_new, initialCondition, options);

    %% Calculate relic density
    Td = mD/xf;      % decoupling temperature
    Yd = Y(end);     % Yield at decoupling

    % Calculate the yield today
    YieldToday = IntegrateTillToday(Td,T0,Yd,R,mD,
csDDnunu_a,csDDnunu_b,csDDZZ_a,csDDZZ_b);

    Oh2 = g_D * mD * YieldToday * s0 / rhoc_h2;
```

GridSearch.m

```matlab
clearvars
clc
format long e

% Add degrees of freedom
addpath bessel degrees_of_freedom
dof
% Start Timer
tic
% Import Constants (MPlank, G, rhoc_h2 ...)
Constants

% Parameters of model
mD      =    100;
g       =    0.1;
g_prime =    g;
% Arrays to loop
gX_array=logspace(-3, log10(0.3), 200);
R_array=linspace(0.5, 4, 200);
% Initialize result matrix and counter
Oh2_array=zeros(length(R_array), length(gX_array));
Zaehler=0;
% Grid search
for n=1:length(R_array)
    R=R_array(n); % Declare R
    for m=1:length(gX_array)
        gX=gX_array(m);  % Declare gX
        MZ=R*mD;
        Oh2Calculator % ODE solver and calculates relic Density
        Oh2_array(n,m)=Oh2; % Save value
        Zaehler=Zaehler+1;
        disp(num2str(Zaehler));
    end
end
%% Code to save file (left out here)
```

```matlab
function [optimizedParameter, finalOh2] = optimizeParameter(
    Parameter, lower_bound, upper_bound, ~, mD, R, g, gX)

%adding paths
addpath bessel degrees_of_freedom
dof

Constants

%Todays relic Density
goal_relic_density = 0.12;
deltaOh2 = 10;
tolerance = 0.01;

tic

switch Parameter

    case 'mD'
        %% Bisection method for finding mD

        i=0; %for counting the interations
        stuckCounter = 0;
        while deltaOh2 > tolerance
            % Choose midpoint
            mD = (lower_bound + upper_bound) / 2;
            MZ = R.*mD;
            g_prime = g;

            Oh2Calculator

            deltaOh2 = abs( Oh2 - goal_relic_density);

            % Bug fixing. If value is stuck at upper or lower
    limit ( 1% margin) after
            % 10 iterations it is just set there.
            if (mD <= lower_bound + 0.01*lower_bound) || (mD >=
     upper_bound-0.01*upper_bound)
                stuckCounter = stuckCounter + 1;
            else
```

```matlab
                stuckCounter = 0;
            end

            if stuckCounter == 15
                deltaOh2 = tolerance/2;
                stuckCounter = 0;
            end

            %% Update bounds
            if Oh2 > goal_relic_density
                upper_bound = mD;
            else
                lower_bound = mD;
            end
            i=i+1;

            disp(['Current mD : ', num2str(mD) ])
            disp(['Current Oh2 : ', num2str(Oh2) ])
            disp(['DeltaOh2 : ', num2str(deltaOh2)])
            disp('-------------------------------------------')

        end

        optimizedParameter=mD;
        finalOh2=Oh2;

%% Cases for the other parameters with the same structure are
    left out
```

OptimizeGridSearch.m

```matlab
clc
clearvars
format long e

addpath bessel degrees_of_freedom
dof

tic

%% Optimal mD for different gX with given g and variing R

% Parameters of model
mD      =    100;   %random Value gets overwritten later
g       =    0.1;
g_prime =    g;
gX      =    0.2;
R       =    1.5;
MZ      =    R.*mD;

R_values = linspace(0.5, 4, 50);

gX_values = logspace(-3, log10(0.3), 50);

optimized_mD_values = zeros(length(R_values),length(gX_values))
    ;
for k = 1:length(R_values)

    R = R_values(k);

    l = 1;

    while l <= length(gX_values)

        gX = gX_values(l);
        disp(['For R: ', num2str(R),' and gX: ', num2str(gX)])
        [mD, Oh2] = optimizeParameter('mD', 0.01, 10000, 0.01,
    mD, R, g, gX);
        optimized_mD_values(k,l) = mD;

        l=l+1;
```

```matlab
39        end
40 end
41
42 toc
43
44 %%Saving the data in txt.file (left out here)
```

References

[1] Daniel Baumann. *Cosmology*. Lecture notes. Science Park, 1090 GL Amsterdam, The Netherlands, 2024.

[2] John T. Thompson. *Dark Matter and Dark Energy Lecture*. Online; Accessed 2024-07-05. 2024. URL: https://www.astronomy.ohio-state.edu/thompson.1847/1101/lecture_darkmatter_darkenergy.html.

[3] Horace W. Babcock. "The rotation of the Andromeda Nebula". In: *Lick Observatory Bulletin No. 498*. University of California Press, 1939.

[4] Stefano Profumo, Luca Giani, and Oliver F. Piattella. "An Introduction to Particle Dark Matter". In: *arXiv preprint* (2019). arXiv: 1910.05610.

[5] ESA/Hubble. *Hubble Captures a Stunning Galactic Crash*. Accessed: 2024-07-05. 2011. URL: https://esahubble.org/images/heic1106c/.

[6] Richard Massey, Thomas Kitching, and Johan Richard. "The dark matter of gravitational lensing". In: (May 2010). arXiv: 1001.1739v2 [astro-ph.CO]. URL: http://arxiv.org/pdf/1001.1739.

[7] Gianfranco Bertone, Dan Hooper, and Joseph Silk. "Particle dark matter: evidence, candidates and constraints". In: *Physics Reports* 405.5 (2005), pp. 279–390. ISSN: 0370-1573. DOI: https://doi.org/10.1016/j.physrep.2004.08.031. URL: https://www.sciencedirect.com/science/article/pii/S0370157304003515.

[8] Gerard Jungman, Marc Kamionkowski, and Kim Griest. "Supersymmetric Dark Matter". In: *Physics Reports* 267 (1996), pp. 195–373. DOI: 10.1016/0370-1573(95)00058-5.

[9] Rebecca K. Leane. "Indirect Detection of Dark Matter in the Galaxy". In: *arXiv preprint* (2020). arXiv: 2006.00513.

[10] Cush and MissMJ. *Standard Model of Elementary Particles*. https://en.wikipedia.org/wiki/File:Standard_Model_of_Elementary_Particles.svg. Released into the public domain by Cush; original version licensed under CC BY 3.0 by MissMJ. 2024.

[11] José Ignacio Illana and Alejandro Jiménez Cano. "Quantum field theory and the structure of the Standard Model". In: *arXiv* (2022). Departamento de Física Teórica y del Cosmos, Universidad de Granada, E-18071 Granada, Spain and Laboratory of Theoretical Physics, Institute of Physics, University of Tartu, 50411 Tartu, Estonia. arXiv: 2211.14636 [hep-th]. URL: http://arxiv.org/pdf/2211.14636.

[12] F. Halzen and A. D. Martin. *Quarks and Leptons: An Introductory Course in Modern Particle Physics*. New York: John Wiley & Sons, 1984.

[13] Max Planck Society. *Neutrinos: grundlegende Erkenntnisse durch rätselhafte Teilchen.* Accessed: 2024-07-06. 2024. URL: https://www.mpg.de/neutrinos-grundlegende-erkenntnisse-durch-raetselhafte-teilchen.

[14] The KATRIN Collaboration. "Direct neutrino-mass measurement with sub-electronvolt sensitivity". In: *Nature Physics* 18 (2022), pp. 160–166. DOI: 10.1038/s41567-021-01463-1. URL: https://doi.org/10.1038/s41567-021-01463-1.

[15] The University of Chicago. *The Hubble Constant, explained.* Accessed: 2024-07-06. 2023. URL: https://news.uchicago.edu/explainer/hubble-constant-explained#what.

[16] European Space Agency. *Planck CMB.* Accessed: 2024-07-06. 2013. URL: https://www.esa.int/ESA_Multimedia/Images/2013/03/Planck_CMB.

[17] Planck Collaboration. "Planck 2018 results. VI. Cosmological parameters". In: *arXiv e-prints* (2018). arXiv: 1807.06209 [astro-ph.CO]. URL: https://arxiv.org/abs/1807.06209.

[18] Paolo Gondolo and Graciela Gelmini. "Cosmic abundances of stable particles: Improved analysis". In: *Nuclear Physics B* 360 (1991), pp. 145–179.

[19] Mirco Cannoni. "Relativistic σv in the calculation of relics abundances: a closer look". In: *arXiv e-prints* (May 2014). (Dated: November 17, 2013). arXiv: 1311.4508v2 [astro-ph.CO]. URL: https://arxiv.org/abs/1311.4508v2.

[20] E. Byckling and K. Kajantie. *Particle Kinematics.* See Chapters 2 and 3. London: John Wiley & Sons Ltd., 1973.

[21] Hartmut Pilkuhn. *The Interaction of Hadrons.* See Chapter 1. Amsterdam: North Holland Publishing Company, 1967.

[22] Michele Maggiore. *A Modern Introduction to Quantum Field Theory.* See Chapter 6. Oxford, UK: Oxford University Press, 2005.

[23] FeynCalc Development Team. *FeynCalc: Mathematica package for symbolic calculations in quantum field theory.* Used with `Mathematica 13`. Version 10.6.0. 2023. URL: http://www.feyncalc.org/.

[24] MathWorks. *MATLAB R2023a Documentation: ode15s.* https://www.mathworks.com/help/matlab/ref/ode15s.html. 2023.

[25] Carlos A. Argüelles et al. "Dark Matter Annihilation to Neutrinos". In: *arXiv e-prints* (June 2021). Version 3. arXiv: 1912.09486v3 [hep-ph]. URL: https://arxiv.org/abs/1912.09486v3.

[26] KM3NeT Collaboration. *KM3NeT Collaboration.* Accessed: 2024-07-06. 2024. URL: https://www.km3net.org/.

[27]   Ronald Kleiss and Hugo Kuijf. "Feynman Diagrams for Beginners". In: *arXiv preprint arXiv:1602.04182* (2016). Notes for the exercises at the Adriatic School on Particle Physics and Physics Informatics, 11–21 Sep 2001, Split, Croatia. URL: https://arxiv.org/pdf/1602.04182.